

# HIFIR: Hybrid Incomplete Factorization with Iterative Refinement for Preconditioning Ill-conditioned and Singular Systems

QIAO CHEN and XIANGMIN JIAO, Stony Brook University, USA

We introduce a software package called *HIFIR* for preconditioning sparse, unsymmetric, ill-conditioned, and potentially singular systems. *HIFIR* computes a *hybrid incomplete factorization*, which combines multilevel incomplete LU factorization with a truncated, rank-revealing QR factorization on the final Schur complement. This novel hybridization is based on the new theory of  $\epsilon$ -accurate approximate generalized inverse. It enables near-optimal preconditioners for consistent systems and enables flexible GMRES to solve inconsistent systems when coupled with iterative refinement. In this paper, we focus on some practical algorithmic and software issues of *HIFIR*. In particular, we introduce a new inverse-based rook pivoting into ILU, which improves the robustness and the overall efficiency for some ill-conditioned systems by significantly reducing the size of the final Schur complement for some systems. We also describe the software design of *HIFIR* in terms of its efficient data structures for supporting rook pivoting in a multilevel setting, its template-based generic programming interfaces for mixed-precision real and complex values in C++, and its user-friendly high-level interfaces in MATLAB and Python. We demonstrate the effectiveness of *HIFIR* for ill-conditioned or singular systems arising from several applications, including the Helmholtz equation, linear elasticity, stationary incompressible Navier–Stokes equations, and time-dependent advection-diffusion equation.

CCS Concepts: • **Mathematics of computing** → **Computations on matrices**; *Solvers*; • **Software and its engineering** → Software libraries and repositories.

Additional Key Words and Phrases: preconditioning, hybrid incomplete factorization, multilevel ILU factorization, rank-revealing factorization, singular systems, approximate generalized inverse, iterative refinement

## ACM Reference Format:

Qiao Chen and Xiangmin Jiao. 2021. HIFIR: Hybrid Incomplete Factorization with Iterative Refinement for Preconditioning Ill-conditioned and Singular Systems. *ACM Trans. Math. Softw.* 1, 1 (December 2021), 32 pages. <https://doi.org/10.1145/nnnnnnn.nnnnnnn>

## 1 INTRODUCTION

We consider the problem of preconditioning an iterative solver for a linear system,

$$Ax = b, \quad (1)$$

where  $A \in \mathbb{C}^{n \times n}$  is sparse and potentially singular,  $x \in \mathbb{C}^n$ , and  $b \in \mathbb{C}^n$ , or as in many applications,  $A \in \mathbb{R}^{n \times n}$ ,  $x \in \mathbb{R}^n$ , and  $b \in \mathbb{R}^n$ . For generality, we will assume complex-valued systems in our discussions. In general, (1) is *inconsistent* in that  $\|b - AA^+b\| \gg \epsilon_{\text{mach}} \|b\|$ , where  $A^+$  denotes the Moore–Penrose pseudoinverse of  $A$  and  $\epsilon_{\text{mach}}$  denotes the

---

Authors' address: Qiao Chen, qiao.chen@stonybrook.edu; Xiangmin Jiao, xiangmin.jiao@stonybrook.edu, Stony Brook University, Department of Applied Mathematics & Statistics and Institute for Advanced Computational Science, Stony Brook, New York, USA, 11794.

---

Permission to make digital or hard copies of all or part of this work for personal or classroom use is granted without fee provided that copies are not made or distributed for profit or commercial advantage and that copies bear this notice and the full citation on the first page. Copyrights for components of this work owned by others than ACM must be honored. Abstracting with credit is permitted. To copy otherwise, or republish, to post on servers or to redistribute to lists, requires prior specific permission and/or a fee. Request permissions from [permissions@acm.org](mailto:permissions@acm.org).

© 2021 Association for Computing Machinery.

Manuscript submitted to ACM

Manuscript submitted to ACM

machine epsilon of a given floating-point number system. In this case, we must seek a *least-squares solution* of (1), i.e.,

$$\mathbf{x}_{LS} = \arg \min_{\mathbf{x}} \|\mathbf{b} - \mathbf{Ax}\|_2, \quad (2)$$

or often preferably the *pseudoinverse solution* of (1), i.e.,

$$\mathbf{x}_{PI} = \arg \min_{\mathbf{x}} \|\mathbf{x}\|_2 \quad \text{subject to} \quad \min \|\mathbf{b} - \mathbf{Ax}\|_2, \quad (3)$$

or equivalently,  $\mathbf{x}_{PI} = \mathbf{A}^+\mathbf{b}$ . When  $\mathbf{A}$  is large-scale, it is preferable to solve (1) using a *Krylov subspace (KSP)* method, such as GMRES [71], which seeks a solution in the  $k$ th KSP

$$\mathcal{K}_k(\mathbf{A}, \mathbf{v}) = \text{span} \left\{ \mathbf{v}, \mathbf{Av}, \dots, \mathbf{A}^{k-1}\mathbf{v} \right\} \quad (4)$$

at the  $k$ th iteration, where  $\mathbf{v}$  is typically equal to  $\mathbf{b}$ . It is well known that KSP methods can benefit from robust and effective preconditioners for ill-conditioned problems. This work introduces a software package called *HIFIR*, which delivers robust and computationally efficient preconditioners for singular systems. As a side product, HIFIR also improves the robustness in preconditioning ill-conditioned systems.

Compared to nonsingular systems, preconditioning (nearly) singular systems is a very challenging problem. Several software packages offer fairly robust and easy-to-use preconditioners for nonsingular systems, such as the multilevel ILU (MLILU) in ILUPACK [15], the supernodal ILU in SuperLU [57], and various parallel preconditioners in PETSc [5]. Conceptually, such software packages construct a preconditioner  $\mathbf{M} \in \mathbb{C}^{n \times n}$  that approximates  $\mathbf{A}$  in that  $\mathbf{M}^{-1} \approx \mathbf{A}^{-1}$ . Given  $\mathbf{M}$ , a right-preconditioned<sup>1</sup> KSP method seeks a solution to

$$\mathbf{AM}^{-1}\mathbf{y} = \mathbf{b} \quad (5)$$

in  $\mathcal{K}_k(\mathbf{AM}^{-1}, \mathbf{v})$ , where typically  $\mathbf{v} = \mathbf{b}$ , and then  $\mathbf{x} = \mathbf{M}^{-1}\mathbf{y}$ . Ideally, the preconditioned KSP methods would converge significantly faster than the unpreconditioned ones. However, when  $\mathbf{A}$  is (nearly) singular and the system (1) is inconsistent, there is a lack of robust algorithms and software. Some earlier techniques used a CGLS-type KSP method (e.g., [14, 30, 64]), which is mathematically equivalent to solving the normal equation using CG [14, 43] or MINRES [30, 63]. Those KSP methods tend to converge slowly due to the squaring of the condition number by the normal equation in the corresponding KSP [48]. More recently, there has been significant interest in preconditioning GMRES-type methods for singular systems or least-squares problems [40, 48, 61]. For example, the so-called AB-GMRES [40] solves the system  $\mathbf{AB}\mathbf{y} = \mathbf{b}$  using GMRES with  $\mathcal{K}_k(\mathbf{AB}, \mathbf{b})$ , and then  $\mathbf{x} = \mathbf{B}\mathbf{y}$ . Here,  $\mathbf{B}$  plays a similar role as  $\mathbf{M}^{-1}$ , except that  $\mathbf{B}$  may be singular (or rank deficient if  $\mathbf{A}$  is rectangular). Hayami et al. [40] constructed  $\mathbf{B}$  based on robust incomplete factorization (RIF) of Benzi and Tuma [11, 12], which was originally developed for CGLS-type methods. Although RIF could accelerate the convergence of AB-GMRES in [40], it was not robust in general [61]. In more recent works [35, 61],  $\mathbf{B}$  in AB-GMRES is typically chosen to be  $\mathbf{A}^H$  (or  $\mathbf{A}^T$  for real matrices), which unfortunately squares the condition number (analogous to CGLS) and in turn can slow down the convergence. This work aims to deliver a right preconditioner that is more efficient and robust than RIF, and more importantly, enables near-optimal convergence rates. We achieve this goal by leveraging the new theory of  $\epsilon$ -accurate approximated generalized inverse (AGI) [48], as outlined in Section 2.

Our development of HIFIR was based on our earlier software package called *HILUCSI* [20], which was a prototype implementation of an MLILU for nonsingular saddle-point problems. Compared to single-level ILUs (such as ILU(k) and

<sup>1</sup>We consider only right preconditioning because left preconditioning alters the computation of residual vector  $\mathbf{r} = \mathbf{b} - \mathbf{Ax}$  and in turn may lead to false stagnation or early terminations for ill-conditioned systems [33].

ILUTP, etc. [70, Chapter 10]), MLILU is generally more robust for nonsingular indefinite systems [20, 33]. HILUCSI leveraged several techniques in a novel way to achieve superior efficiency and robustness for saddle-point problems than other MLILU libraries (such as ARMS [72], ILUPACK [15], and ILU++ [60]). In particular, HILUCSI achieved high efficiency by introducing a scalability-oriented dropping in a dual-thresholding strategy in the fan-in ILU<sup>2</sup> for linear-time complexity in its factorization and solve. It improved robustness by leveraging mixed symmetric and unsymmetric preprocessing techniques at different levels and combining static and dynamic permutations. HIFIR inherits some of these core algorithmic components of HILUCSI, as described in Section 3. However, as an MLILU technique, HILUCSI was not robust for singular systems, for example, when its final level is singular. HIFIR is designed to overcome this deficiency by leveraging a rank-revealing factorization in its final level, introducing iterative refinement to build a variable preconditioner, and introducing a new pivoting strategy in its ILU portion, as we will detail in Section 3.

The main contributions of this work are as follows. First and foremost, we introduce one of the first software libraries to improve the robustness for ill-conditioned and (nearly) singular systems to achieve near machine precision. Our software library, called HIFIR, or *Hybrid Incomplete Factorization with Iterative Refinement*, computes an AGI [48] by hybridizing incomplete LU and rank-revealing QR (RRQR) in a multilevel fashion. When used as a right-preconditioner for GMRES, this hybridization enables (near) optimal convergence for consistent or ill-conditioned systems. When fortified with iterative refinement in FGMRES [69], HIFIR enables the robust computation of the left null space and the pseudoinverse solution of inconsistent systems. We have implemented HIFIR using template-based objective-oriented programming in C++. For user-friendliness, the C++ HIFIR library is header-only, with easy-to-use high-level interfaces in MATLAB and Python. The software is open-source and has been made available at <https://github.com/hifirworks/hifir>. Second, this work also introduces a novel inverse-based rook pivoting (IBRP) in the fan-in ILU. We describe efficient data structures for the efficient implementation of IBRP and show that this new pivoting strategy improves the robustness and efficiency for some challenging singular systems. Third, HIFIR offers some advanced features, such as the support of complex arithmetic, the ability to precondition both  $A$  and  $A^H$  using the same factorization, and the ability to multiply by an AGI of the preconditioning operator. These features enable the use of HIFIR as building blocks for advanced preconditioners, such as (parallel) block preconditioners. In addition, HIFIR supports mixed precision (e.g., double precision combined with single or potentially half precision) for the input matrix and the preconditioner, which is beneficial for heterogeneous hardware platforms and limited-memory settings.

The remainder of this paper is organized as follows. In Section 2, we give an overview of the theoretical foundation of HIFIR, including optimality conditions, treatment for singular systems, etc. In Section 3, we describe the algorithmic components of HIF and highlight some implementation details. Section 4 describes how to apply HIF as a preconditioner, including iterative refinement. In Section 5, we introduce the application programming interfaces of HIFIR in C++, MATLAB, and Python with example implementations. Section 6 demonstrates HIFIR for some large-scale applications with indefinite ill-conditioned and singular inconsistent systems. Finally, Section 7 concludes the paper with a discussion on future directions. For completeness, we present the details of our data structures in Appendix A and the complexity analysis of IBRP in Appendix B.

<sup>2</sup>The technique is also known as the Crout version of ILU [55] or left-looking [27], but we adopt the terminology of “fan in” update, which is commonly used in parallel computing [25] and is more suggestive in terms of its algorithmic behavior.

## 2 THEORETICAL FOUNDATIONS

In this section, we give an overview of the theoretical foundations of HIFIR. Most of the theory was based on that in [48], except that we generalize the results from real matrices to complex ones. We present some of the most relevant theoretical results for completeness, but we omit the proofs because they follow the same arguments as those in [48].

### 2.1 Mathematically optimal right-preconditioning operators for consistent systems

Let us first consider the issue of optimal preconditioning for a consistent system (1), where  $\mathbf{b}$  is in the range of  $\mathbf{A}$  (i.e.,  $\mathbf{b} \in \mathcal{R}(\mathbf{A})$ ). In floating-point arithmetic, the convergence rate of a KSP method for such systems depends on the following generalized notion of condition numbers.

**Definition 1.** Given a potentially singular matrix  $\mathbf{A} \in \mathbb{C}^{m \times n}$ , the *2-norm condition number* of  $\mathbf{A}$  is the ratio between the largest and the smallest nonzero singular values of  $\mathbf{A}$ , i.e.,  $\kappa(\mathbf{A}) = \sigma_1(\mathbf{A})/\sigma_r(\mathbf{A})$ , where  $r = \text{rank}(\mathbf{A})$ .

To accelerate a KSP method for such a system, we solve a right-preconditioned system

$$\mathbf{A}\mathbf{G}\mathbf{y} = \mathbf{b}, \quad (6)$$

using a KSP method, and then  $\mathbf{x} = \mathbf{G}\mathbf{y}$ . We refer to  $\mathbf{G}$  as a *right preconditioning operator (RPO)*. Ideally, we would like  $\kappa(\mathbf{A}\mathbf{G}) \ll \kappa(\mathbf{A})$ . For nonsingular systems,  $\mathbf{G}$  is equivalent to  $\mathbf{M}^{-1}$  in (5); for singular systems,  $\mathbf{G}$  generalizes  $\mathbf{M}^{-1}$ . The symbol  $\mathbf{G}$  signifies that it is based on a *generalized inverse*.

**Definition 2.** [67, Definitions 2.2] Given a potentially rank-deficient  $\mathbf{A} \in \mathbb{C}^{m \times n}$ ,  $\mathbf{A}^g$  is a *generalized inverse* of  $\mathbf{A}$  if and only if  $\mathbf{A}\mathbf{A}^g\mathbf{A} = \mathbf{A}$ .

It is worth noting that the Moore–Penrose pseudoinverse  $\mathbf{A}^+$  is a special case of generalized inverses. Although it might be tempting to construct the RPO  $\mathbf{G}$  to approximate  $\mathbf{A}^+$ , the pseudoinverse is overly restrictive. The following two properties of generalized inverses make them particularly relevant to right-preconditioning singular systems.

**Proposition 1.** [48, Proposition 3.4] If  $\mathbf{A}^g$  is a generalized inverse of  $\mathbf{A} \in \mathbb{C}^{m \times n}$ , then  $\mathbf{A}\mathbf{A}^g$  is diagonalizable, and its eigenvalues are all zeros and ones. In other words, there exists a nonsingular matrix  $\mathbf{X} \in \mathbb{C}^{m \times m}$ , such that  $\mathbf{A}\mathbf{A}^g = \mathbf{X} \begin{bmatrix} \mathbf{I}_r & \\ & 0 \end{bmatrix} \mathbf{X}^{-1}$ , where  $\mathbf{I}_r$  is the  $r \times r$  identity matrix with  $r = \text{rank}(\mathbf{A})$ . Conversely, if there exists a nonsingular  $\mathbf{X}$  such that  $\mathbf{A}\mathbf{G} = \mathbf{X} \begin{bmatrix} \mathbf{I}_r & \\ & 0 \end{bmatrix} \mathbf{X}^{-1}$  for  $r = \text{rank}(\mathbf{A})$ , then  $\mathbf{G}$  is a generalized inverse of  $\mathbf{A}$ .

**Proposition 2.** [48, Proposition A.1] Given  $\mathbf{A} \in \mathbb{C}^{n \times n}$  of rank  $r = \text{rank}(\mathbf{A})$  and a generalized inverse  $\mathbf{A}^g$  with  $\mathbf{A}\mathbf{A}^g = \mathbf{X} \begin{bmatrix} \mathbf{I}_r & \\ & 0 \end{bmatrix} \mathbf{X}^{-1}$ , the condition number of  $\mathbf{A}\mathbf{A}^g$  is bounded by  $\kappa(\mathbf{X})$ , i.e.,  $\kappa(\mathbf{A}\mathbf{A}^g) \leq \kappa(\mathbf{X})$ .

From Proposition 1, it is easy to show that any generalized inverse  $\mathbf{A}^g$  (or a nonzero scalar multiple of  $\mathbf{A}^g$ ) enables a mathematically optimal RPO for consistent systems in the following sense.

**Theorem 1.** [48, Theorem 3.6] Given  $\mathbf{A} \in \mathbb{C}^{n \times n}$  and a generalized inverse  $\mathbf{A}^g$ , then GMRES with RPO  $\alpha\mathbf{A}^g$  with  $\alpha \neq 0$  converges to a least-squares solution  $\mathbf{x}_{LS}$  of (1) after one iteration for all  $\mathbf{b} \in \mathcal{R}(\mathbf{A})$  and  $\mathbf{x}_0 \in \mathbb{C}^n$ . Conversely, if GMRES with RPO  $\mathbf{G}$  converges to a least-squares solution  $\mathbf{x}_{LS}$  in one iteration for all  $\mathbf{b} \in \mathcal{R}(\mathbf{A})$  and  $\mathbf{x}_0 \in \mathbb{C}^n$ , then  $\mathbf{G}$  is a scalar multiple of a generalized inverse of  $\mathbf{A}$ .

A corollary of Theorem 1 is that if  $\mathcal{R}(A^g) = \mathcal{R}(A^H)$ , then the computed  $\mathbf{x}_{LS}$  is the pseudoinverse solution of (1). Let  $\Pi_{\mathcal{R}(A^H)}$  denote a projection onto  $A^H$ . Given any  $A^g$ , it is easy to show that  $\Pi_{\mathcal{R}(A^H)} A^g$  is also a generalized inverse, and the computed  $\mathbf{x}_{LS}$  with  $\Pi_{\mathcal{R}(A^H)} A^g$  as the RPO is then the pseudoinverse solution. Theorem 1 assumes exact arithmetic. With rounding errors, the condition number of  $AA^g$  must be bounded by a small constant, which holds in general if  $\kappa(X)$  is bounded due to Proposition 2.

Although the above theory may seem abstract, it suggests a new approach for constructing RPO based on generalized inverses. In particular, one option to construct  $A^g$  is to hybridize multilevel ILU with a rank-revealing decomposition on its final Schur complement. As an illustration, consider the following example that combines LU factorization without pivoting with QR factorization with column pivoting (QRCP) [34].

**Example 1.** Given  $A \in \mathbb{C}^{n \times n}$ , after  $n_1$  steps of Gaussian elimination,

$$A = \begin{bmatrix} L_1 & \\ L_2 & I_{n_2} \end{bmatrix} \begin{bmatrix} I_{n_1} & \\ & S \end{bmatrix} \begin{bmatrix} U_1 & U_2 \\ & I_{n_2} \end{bmatrix}, \quad (7)$$

where  $S \in \mathbb{C}^{n_2 \times n_2}$  is the *Schur complement*. Clearly,  $\text{rank}(A) = n_1 + \text{rank}(S)$ . Let the QRCP of  $S$  be

$$SP = Q \begin{bmatrix} R_1 & R_2 \\ & 0 \end{bmatrix}, \quad (8)$$

where  $Q \in \mathbb{C}^{n_2 \times n_2}$  is unitary and  $R_1 \in \mathbb{C}^{s \times s}$  for  $s = \text{rank}(S)$  (i.e., the (numerical) rank of  $S$ ). Let  $\hat{P}$  and  $\hat{Q}$  be composed of the first  $s$  columns of  $P$  and  $Q$ , respectively. Then,  $S^g = \hat{P}R_1^{-1}\hat{Q}^H$  is a generalized inverse of  $S$  with  $SS^H = \hat{Q}\hat{Q}^H = QI_sQ^H$ . Furthermore,

$$G = \begin{bmatrix} U_1 & U_2 \\ & I_{n_2} \end{bmatrix}^{-1} \begin{bmatrix} I_{n_1} & \\ & S^g \end{bmatrix} \begin{bmatrix} L_1 & \\ L_2 & I_{n_2} \end{bmatrix}^{-1} = \begin{bmatrix} U_1 & U_2 \\ & I_{n_2} \end{bmatrix}^{-1} \begin{bmatrix} I_{n_1} & \\ & P \begin{bmatrix} R_1^{-1} & 0 \\ & 0 \end{bmatrix} Q^H \end{bmatrix} \begin{bmatrix} L_1 & \\ L_2 & I_{n_2} \end{bmatrix}^{-1} \quad (9)$$

is a generalized inverse of  $A$ , with  $X = \begin{bmatrix} L_1 & \\ L_2 & I_{n_2} \end{bmatrix} \begin{bmatrix} I_{n_1} & \\ & Q \end{bmatrix}$  for  $X$  as in Proposition 1.

We refer to the preceding construction of  $G$  as a *hybrid factorization*. It enables a more efficient approach to construct an optimal RPO, for example, compared to applying QRCP to  $A$  if  $n_2 \ll n$ . For the strategy to be successful, we must address some practical issues. First, we need to allow droppings in the factorization to reduce computational cost and memory requirement, especially for larger-scale systems. Second, we need to control  $\kappa \left( \begin{bmatrix} L_1 & \\ L_2 & I \end{bmatrix} \right)$  to limit  $\kappa(AG)$ , for example, by leveraging pivoting and equilibration [26]. Third, it is desirable to make  $S$  as small as possible before we apply QRCP. Hereafter, we will address the first two issues from a theoretical perspective and then address the third issue in Section 3.

## 2.2 Near-optimal right-preconditioning operators via approximate generalized inverses

Although a mathematically optimal RPO enables the most rapid convergence of KSP methods, the computational cost per iteration may be prohibitively high, so is the memory requirement. In practice, it may be more desirable to construct “near-optimal” RPOs by approximating a generalized inverse. The following definition and theorem establish the guideline for constructing such approximations.

**Definition 3.** [48, Definition 3.8] Given  $A \in \mathbb{C}^{n \times n}$ ,  $G$  is an  $\epsilon$ -accurate approximate generalized inverse (AGI) if there exists  $X \in \mathbb{C}^{n \times n}$  such that

$$\left\| X^{-1} A G X - \begin{bmatrix} I_r & \\ & 0 \end{bmatrix} \right\| = \epsilon \leq 1, \quad (10)$$

where  $I_r$  is  $r \times r$  identity matrix with  $r = \text{rank}(A)$ . A class of AGI is  $\epsilon$ -accurate if  $\epsilon$  tends to 0 as its control parameters are tightened.  $G$  is a stable AGI if  $\kappa(X) \leq C$  for some  $C \ll 1/\epsilon_{\text{mach}}$ .

**Theorem 2.** [48, Theorem 3.9] GMRES with an  $\epsilon$ -accurate AGI  $G$  of  $A$  converges to a least-squares solution  $\mathbf{x}_{LS}$  of (1) in exact arithmetic for all consistent systems (i.e.,  $\mathbf{b} \in \mathcal{R}(A)$ ) with any initial guess  $\mathbf{x}_0 \in \mathbb{C}^n$ .

A corollary of Theorem 2 is that given an  $\epsilon$ -accurate AGI  $G$ ,  $\Pi_{\mathcal{R}(A^H)} G$  is also an  $\epsilon$ -accurate AGI, and the computed  $\mathbf{x}_{LS}$  with  $\Pi_{\mathcal{R}(A^H)} G$  as the RPO is the pseudoinverse solution. Mathematically, it is equivalent to compute  $\mathbf{x}_{LS}$  with  $G$  as the RPO and then project  $\mathbf{x}_{LS}$  onto  $\mathcal{R}(A^H)$  to obtain the pseudoinverse solution.

*Remark 1.* In the literature, commonly used measures of accuracy and stability of a preconditioner  $M$  for a nonsingular matrix  $A$  were  $\|A - M\|_F$  and  $\|I - AM^{-1}\|_F$ , respectively; see, e.g., [8]. Our new definitions of accuracy and stability in Definition 3 are more general in that they apply to singular systems. In addition, they are more rigorous in that they are based on Theorem 2 and Proposition 2, respectively, instead of based on empirical evidence [8].

Theorem 2 and Example 1 suggest that we can construct AGIs by replacing the LU factorization in hybrid factorization with some ILU variants. We will refer to the combination of ILU with a rank-revealing factorization on the Schur complement as a *hybrid incomplete factorization (HIF)*. From the perspective of AGI, a good candidate ILU should satisfy three critical criteria. First, the ILU needs to have prudent dropping strategies to make the approximation as accurate as possible. Second, we must be able to control  $\kappa(AG)$  effectively for stability. Third, the computational cost and storage requirement should ideally scale linearly (or near-linearly) with respect to the input size. In the ILU literature [16, 22, 70], there had been significant attention to the first criterion. However, the second criterion excludes simple ILU techniques without pivoting, such as ILU(k) [70]. The third criterion excludes ILU with relatively simple pivoting strategies, such as ILUTP [22, 70] and its supernodal variants [57], which suffer from superlinear complexity [20, 33].

Although the second and third criteria may appear self-contradicting for traditional ILU techniques, they can be met by a well-designed MLILU technique. Before delving into the details of MLILU algorithms, let us briefly review MLILU and more importantly, show that MLILU can be used to construct accurate and stable AGIs. First, consider a two-level ILU (or more precisely, ILDU) of  $A \in \mathbb{C}^{n \times n}$ ,

$$P^T W A V Q = \begin{bmatrix} B & F \\ E & C \end{bmatrix} \approx \tilde{M} = \begin{bmatrix} \tilde{B} & \tilde{F} \\ \tilde{E} & C \end{bmatrix} = \begin{bmatrix} L_B & \\ & I \end{bmatrix} \begin{bmatrix} D_B & \\ & S \end{bmatrix} \begin{bmatrix} U_B & U_F \\ & I \end{bmatrix}, \quad (11)$$

where  $B \approx \tilde{B} = L_B D_B U_B$  is an ILDU of the leading block,  $E \approx \tilde{E} = L_E D_B U_B$ ,  $F \approx \tilde{F} = L_B D_B U_F$ , and

$$S = C - \tilde{E} \tilde{B}^{-1} \tilde{F} = C - L_E D_B U_F \quad (12)$$

is the Schur complement;  $P$  and  $Q$  are row and column permutation matrices, respectively;  $W$  and  $V$  correspond to row and column scaling diagonal matrices, respectively. The Schur complement  $S$  can be factorized recursively using the same ILU technique, leading to an  $m$ -level ILU preconditioners, namely,

$$M = \underbrace{W_1^{-1} P_1 L_1 \cdots W_m^{-1} P_m L_m}_L \begin{bmatrix} D \\ S_m \end{bmatrix} \underbrace{U_m Q_m^T V_m^{-1} \cdots U_1 Q_1^T V_1^{-1}}_U, \quad (13)$$

where  $L_i = \begin{bmatrix} I_{n-n_i} & & \\ & L_B^{(i)} & \\ & L_E^{(i)} & I \end{bmatrix} \in \mathbb{C}^{n \times n}$  for  $\begin{bmatrix} L_B^{(i)} & \\ L_E^{(i)} & I \end{bmatrix} \in \mathbb{C}^{n_i \times n_i}$  in (11) at the  $i$ th level (similarly for  $U_i$  and all other permutation and scaling matrices),  $D$  is composed of the “union” of  $D_B$  in (11) for all levels, and  $S_m$  is the final Schur complement. As in Example 1, we apply QRCP to  $S_m$  to obtain  $S_m P = Q \begin{bmatrix} R_1 & R_2 \\ & 0 \end{bmatrix}$ , where  $Q \in \mathbb{C}^{n_m \times n_m}$  is unitary and  $R_1 \in \mathbb{C}^{n_s \times n_s}$  with  $n_s = \text{rank}(S_m)$ ,  $r_{11} \geq r_{22} \geq \dots \geq r_{n_s n_s} > 0$  along its diagonal, and  $\kappa(R_1) \ll 1/\epsilon_{\text{mach}}$ . We define an RPO as

$$G = U^{-1} \begin{bmatrix} D^{-1} & \\ & S_m^g \end{bmatrix} L^{-1} = U^{-1} \begin{bmatrix} D^{-1} & \\ & P \begin{bmatrix} R_1^{-1} & 0 \\ & 0 \end{bmatrix} Q^H \end{bmatrix} L^{-1}, \quad (14)$$

where  $L$ ,  $U$ , and  $D$  are as in (13). We note the following fact.

**Proposition 3.** [48, Lemma 4.3] *If no dropping is applied in MLILU, then  $G$  in (14) is a generalized inverse of  $A$  with  $X = L \begin{bmatrix} I_{n-n_m} & \\ & Q \end{bmatrix}$  for  $X$  as in Proposition 1.*

Since  $G$  without dropping is an optimal RPO for consistent systems due to Theorem 1, we claim that an  $\epsilon$ -accurate and stable  $G$  constitutes a near-optimal RPO for consistent systems. The near optimality requires sufficient small droppings and numerical stability, or more precisely,  $X^{-1}AGX$  should be close to  $\begin{bmatrix} I_r & \\ & 0 \end{bmatrix}$  for  $r = \text{rank}(A)$  and  $\kappa(L)$  must be controlled by the algorithm. To this end, we utilize an MLILU technique called *HILUCSI*, which stands for *Hierarchical Incomplete LU-Crout with Scalability-oriented and Inverse-based droppings* [20]. HILUCSI leverages several techniques, including fan-in ILU [55], equilibration [26], static and dynamic pivoting across different levels [16, 20], etc., to meet the accuracy and stability requirements. As the name suggests, HILUCSI focuses on scalability in terms of problem sizes, and it has linear time complexity in each level for both the factorization and solve stages [20]. We defer the detailed description of these algorithmic components to Section 3.

*Remark 2.* Besides HILUCSI, there were several MLILU software packages, such as ARMS [72], ILU++ [59], ILUPACK [15], etc. Proposition 3 can also be applied to improve those packages to solve singular systems by applying QRCP to the final Schur complement. To harness this benefit, however, one must also extend them (especially ARMS and ILU++) to ensure the stability of the  $L$  factor.

Finally, we note that it is sometimes needed to reuse HIF to construct preconditioners for both  $A$  and  $A^H$ . To achieve, we note the following property:

**Proposition 4.** [48, Proposition 3.5] *If  $A^g$  is a generalized inverse of  $A \in \mathbb{C}^{m \times n}$ , then  $A^{gH} \equiv (A^g)^H$  is a generalized inverse of  $A^H$ .*

Conceptually, we can extend (11) to construct a preconditioner  $\tilde{M}^H$  for  $A^H$  as

$$Q^T V A^H W P \approx \tilde{M}^H = \begin{bmatrix} \tilde{B}^H & \tilde{E}^H \\ \tilde{F}^H & C^H \end{bmatrix} = \begin{bmatrix} U_B^H & \\ U_F^H & I \end{bmatrix} \begin{bmatrix} \bar{D}_B & \\ & S^H \end{bmatrix} \begin{bmatrix} L_B^H & L_E^H \\ & I \end{bmatrix}. \quad (15)$$

### 2.3 Variable preconditioning via iterative refinement for null-space computation

The preceding discussions focused on consistent systems. For inconsistent systems, i.e.,  $\mathbf{b} \in \mathbb{C}^n \setminus \mathcal{R}(\mathbf{A})$ , an AGI (or even a generalized inverse<sup>3</sup>) cannot guarantee the convergence of GMRES due to the following fact.

**Theorem 3.** [48, Theorem 2.4] *GMRES with RPO  $\mathbf{G}$  does not break down until finding a least-squares solution  $\mathbf{x}_{LS}$  of (1) for all  $\mathbf{b} \in \mathbb{C}^n$  and  $\mathbf{x}_0 \in \mathbb{C}^n$  if and only if  $\mathbf{AG}$  is range symmetric (i.e.,  $\mathcal{R}(\mathbf{AG}) = \mathcal{R}((\mathbf{AG})^H)$ ) and  $\mathcal{R}(\mathbf{A}) = \mathcal{R}(\mathbf{AG})$ . Furthermore,  $\mathbf{x}_{LS}$  is the pseudoinverse solution if  $\mathcal{R}(\mathbf{G}) = \mathcal{R}(\mathbf{A}^H)$ .*

*Remark 3.* The main challenge posed by Theorem 3 is that it is difficult, if not impossible, to ensure the range symmetry of  $\mathbf{AG}$  for an approximate generalized inverse  $\mathbf{G}$ . The requirement of range symmetry is the primary reason why  $\mathbf{A}^H$  is often used as  $\mathbf{B}$  in AB-GMRES [35, 61]. It is also a key factor for the prevalence of CGLS-type KSP methods [14, 30, 64] for solving singular and least-squares problems. Although such methods can be accelerated by applying some preconditioners, such as incomplete QR [47, 68] or RIF [11, 12], it is difficult for these preconditioners to overcome the slowdown caused by the squaring of the condition number by the normal equation.

Fortunately, this issue can be resolved by using flexible GMRES with *variable preconditioners*, as formalized by the following definition and theorem.

**Definition 4.** [48, Definition 2.1] Given a matrix  $\mathbf{A} \in \mathbb{C}^{n \times n}$ , an initial vector  $\mathbf{v} \in \mathbb{C}^n$ , and variable preconditioners  $\mathcal{G}_{k-1} = [\mathcal{G}_1, \mathcal{G}_2, \dots, \mathcal{G}_{k-1}]$ , the  $k$ th *flexible Krylov subspace (FKSP)* associated with  $\mathbf{A}$ ,  $\mathbf{v}$ , and  $\mathcal{G}_{k-1}$  is

$$\mathcal{K}_k(\mathbf{A}, \mathbf{v}, \mathcal{G}_{k-1}) = \text{span}\{\mathbf{v}, \mathbf{A}\mathcal{G}_1(\mathbf{v}_1), \dots, \mathbf{A}\mathcal{G}_{k-1}(\mathbf{v}_{k-1})\}, \quad (16)$$

where  $\mathbf{v}_{k-1} \in \mathcal{K}_{k-1}(\mathbf{A}, \mathbf{v}, \mathcal{G}_{k-2}) \setminus \{0\}$  and  $\mathbf{v}_{k-1} \perp \mathcal{K}_{k-2}(\mathbf{A}, \mathbf{v}, \mathcal{G}_{k-3})$  for  $k \geq 2$ . The *flexible Krylov matrix*, denoted by  $\mathbf{K}_k$ , is composed of the basis vectors in (16).

The orthogonality of  $\mathbf{v}_{k-1}$  with  $\mathcal{K}_{k-2}(\mathbf{A}, \mathbf{v}, \mathcal{G}_{k-3})$  can be enforced using a generalization of Arnoldi iterations as in [69].

**Theorem 4.** [48, Theorem 2.5] *If FGMRES with variable preconditioners  $\mathcal{G} = [\mathcal{G}_1, \mathcal{G}_2, \dots]$  does not break down until step  $k+1$ , where  $k = \text{rank}(\mathbf{A})$  for a specific  $\mathbf{b} \in \mathcal{R}(\mathbf{A})$  and  $k = \text{rank}(\mathbf{A}) + 1$  for  $\mathbf{b} \in \mathbb{C}^n \setminus \mathcal{R}(\mathbf{A})$ , respectively. If  $\mathcal{R}(\mathbf{A}) = \sum_{i=1}^k \mathcal{R}(\mathbf{A}\mathcal{G}_i)$ , then it finds a least-squares solution of (1) for an initial guess  $\mathbf{x}_0 \in \mathbb{C}^n$ .*

One effective approach to construct variable preconditioners is to introduce *iterative refinement (IR)* in HIF, leading to HIFIR. Specifically, given an  $\epsilon$ -accurate AGI  $\mathbf{G}$  and an initial vector  $\mathbf{v}_0 \in \mathbb{C}^n$  (typically,  $\mathbf{v}_0 = 0$ ), we refine the solution of  $\mathbf{A}\mathbf{v} = \mathbf{q}$  iteratively by obtaining  $\mathbf{v}_j$  for  $j = 1, 2, \dots$  as

$$\mathbf{v}_j = (\mathbf{I} - \mathbf{GA})\mathbf{v}_{j-1} + \mathbf{Gq}. \quad (17)$$

Eq. (17) defines the  $i$ th RPO  $\mathcal{G}_i$  in  $\mathcal{G}$ , and different  $\mathcal{G}_i$  may use different numbers of IR iterations. Note that (17) in general does not converge by a standalone iterative solver in that  $\rho(\mathbf{I} - \mathbf{GA}) \geq 1$  when  $\mathbf{G}$  is a generalized inverse, and Eq. (17) cannot introduce additional nonlinearity into the variable preconditioner  $\mathcal{G}$  and in turn undermine the robustness of FGMRES due to Theorem 4. Hence, we shift our attention to its use as a variable preconditioner in the context of computing null-space vectors. In particular, we apply the technique to compute the left null space of  $\mathbf{A}$  (i.e.,  $\mathcal{N}(\mathbf{A}^H)$ ), which allows us to convert an inconsistent system into a consistent one. Furthermore, by applying the same

<sup>3</sup>When  $\mathbf{G} = \mathbf{A}^g$ , then right-preconditioned GMRES converges to a weighted-least-squares (WLS) solution for inconsistent systems, instead of least-squares solution [48, Theorem 3.7]. We cannot convert the WLS solution into a pseudoinverse solution by projecting it onto  $\mathcal{R}(\mathbf{A}^H)$ .



technique to compute the right null space of  $A$  (i.e.,  $\mathcal{N}(A)$ ), we can convert a least-squares solution from the consistent system into the pseudoinverse solution [48].

### 3 RECURSIVE CONSTRUCTION OF HYBRID INCOMPLETE FACTORIZATION

In this section, we describe the overall algorithm for constructing HIF. Similar to that of HILUCSI [20] and other MLILU algorithms, HIF is a recursive algorithm. As shown in Figure 1, at each level, HIF takes an input matrix  $A$ . HIF first performs symmetric or unsymmetric preprocessing depending on whether  $A$  is (nearly) pattern symmetric, i.e.,  $\text{nnp}(A) \approx \text{nnp}(A^T)$ ; see Section 3.4. The process leads to  $\hat{P}^T W A V \hat{Q} = \hat{P}^T \hat{A} \hat{Q}$ , where  $\hat{P}$ ,  $W$ ,  $V$ , and  $\hat{Q}$  are obtained from preprocessing. If  $A$  is nearly pattern symmetric, the preprocessing step may involve static deferring, which splits  $\hat{P}^T \hat{A} \hat{Q}$  into a 2-by-2 block matrix, i.e.,  $\hat{P}^T \hat{A} \hat{Q} = \begin{bmatrix} \hat{B} & \hat{F} \\ \hat{E} & \hat{C} \end{bmatrix}$ . Depending on whether the leading block  $\hat{B}$  is Hermitian, we then perform incomplete  $LDL^H$  or  $LDU$  factorizations, respectively, where  $L$  and  $U$  are unit lower and upper triangular matrices, respectively (i.e., their diagonal entries are ones). We compute these factorizations using *fan-in updates* (aka the Crout version of ILU), which update the  $k$ th column of  $L$  using columns 1 through  $k - 1$  and update the  $k$ th row of  $U$  using rows 1 through  $k - 1$  at the  $k$ th step, respectively. For stability, we combine fan-in updates with dynamic deferring and scalability-oriented droppings; see Section 3.1. In addition, HIF enables rook pivoting when the previous level had too many deferrals as indicated by the Boolean tag *ibrp* in Figure 1; see Section 3.2. The dynamic deferring may permute some rows and columns in  $\hat{B}$  after  $\hat{E}$  and  $\hat{F}$  to obtain a new 2-by-2 block structure  $\begin{bmatrix} \tilde{B} & \tilde{F} \\ \tilde{E} & \tilde{C} \end{bmatrix}$ , where  $\tilde{E}$  and  $\tilde{F}$  are the leading rows and blocks in  $E$  and  $F$ , respectively. We then compute the Schur complement  $S$  corresponding to  $C$  and factorize  $S$  either directly using RRQR or recursively using HIF, depending on whether  $S$  is sufficiently small or nearly dense; see Section 3.3. Some of the components above are the same as those in HILUCSI [20], the predecessor of HIF. The key differences between HIF and HILUCSI are that 1) HIF introduces a variant of the rook pivoting [66] to improve the stability of ILU and in turn, reduces the size of the final Schur complement  $S_m$  and 2) HIF uses a rank-revealing QR factorization [18] on  $S_m$ . In the following, we first focus on these two aspects and then briefly outline the other components. We will describe how to apply HIF as a preconditioner in Section 4.

#### 3.1 Incomplete $LDU$ with dynamic deferring and scalability-oriented and inverse-based droppings

The core of HIF at each level is incomplete  $LDU$  factorization, or its variant of incomplete  $LDL^H$  factorization. For robustness, we leverage the fan-in ILU, scalability-oriented dropping, inverse-based dropping, and dynamic deferring, as shown in Algorithm 1. Hereafter, we outline the dual thresholding and dynamic deferring steps in fan-in ILU. An optional step in Algorithm 1 is the inverse-based rook pivoting activated by the Boolean flag *ibrp*. We will dedicate Section 3.2 to this new pivoting strategy.

In Algorithm 1, the input matrix  $\hat{A} = W A V$  is obtained from applying preprocessing techniques on either the input matrix  $A$  or the Schur complement from the previous level. Note that in the actual implementation, we do not form  $\hat{A}$  explicitly; instead, we rescale the entries in  $A$  by  $W$  and  $V$  in a “just-in-time” fashion. The procedure `ilu_factorize` also takes  $\hat{P}$  and  $\hat{Q}$  as input, which were obtained from preprocessing along with  $W$  and  $V$  (see Figure 1 and Section 3.4). The main loop in Algorithm 1 factorizes  $\hat{B}$ , the leading block of  $\hat{A}$ , using fan-in ILU similar to those in [54, 55], which delays the computation of the Schur complement as late as possible. Unlike [54, 55], however, `ilu_factorize` dynamically

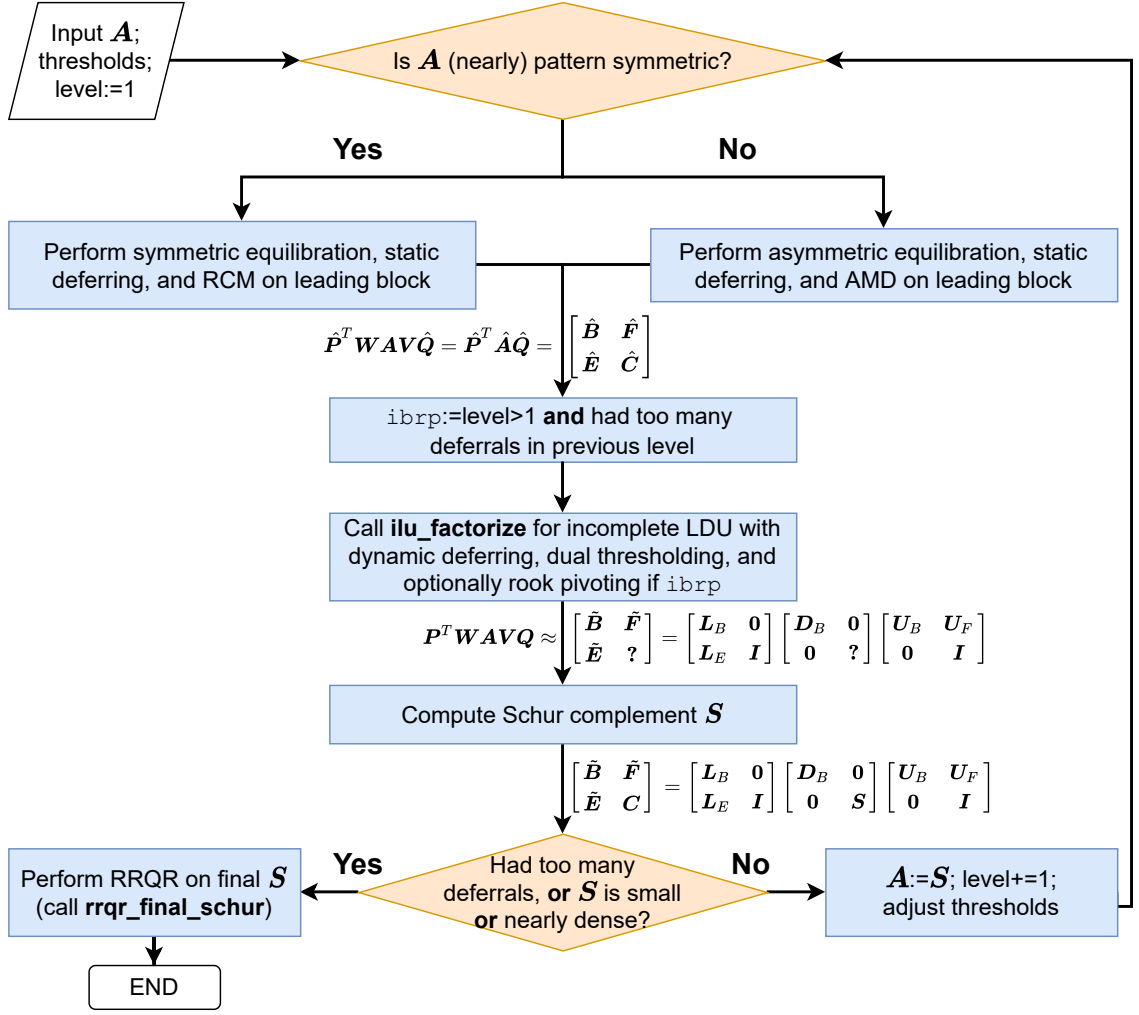


Fig. 1. Overall control flow of hybrid incomplete factorization.

permutes (aka *defers*) rows and columns in  $\hat{B}$  to the end of  $\hat{E}$  and  $\hat{F}$ . The procedure computes

$$P^T W A V Q \approx \begin{bmatrix} \tilde{B} & \tilde{F} \\ \tilde{E} & ? \end{bmatrix} = \begin{bmatrix} L_B & \\ & L_E \end{bmatrix} \begin{bmatrix} D_B & \\ & ? \end{bmatrix} \begin{bmatrix} U_B & U_F \\ & I \end{bmatrix}, \quad (18)$$

where the first and second question marks (“?”) in (18) correspond to  $C$  and  $S$ , which we will describe their computations in Section 3.3. Algorithm 1 returns  $L_B$ ,  $D_B$ ,  $U_B$ ,  $L_E$ ,  $U_F$ ,  $P$ , and  $Q$ , from which  $\tilde{E}$  and  $\tilde{F}$  (along with  $C$ ) can be computed.

A noteworthy feature of **ilu\_factorize** is its *scalability-oriented dropping*, which differs from the dropping strategies in [54, 55] and [15]. Consider the step  $k$  of ILU at a particular level. Using the MATLAB’s colon notation, let  $\ell_{k+1:n,k}$  and  $u_{k,k+1:n}$  denote the  $k$ th column and row of  $\begin{bmatrix} L_B \\ L_E \end{bmatrix}$  and  $\begin{bmatrix} U_B & U_F \end{bmatrix}$ , respectively. Our dropping strategy limits  $\text{nnz}(\ell_{k+1:n,k})$  and  $\text{nnz}(u_{k,k+1:n})$  to be proportional to numbers of nonzeros in the corresponding column and row of

---

**Algorithm 1** `ilu_factorize`( $\hat{A}, p, q, n_1, \text{params}, \text{level}, \text{ibrp}, \text{nr}, \text{nc}$ )

---

**inputs:**

$\hat{A}$ : input scaled matrix of size  $n \times n$  (i.e.,  $\hat{A} = WAV$ , passed in as  $A, W$ , and  $V$  separately)  
 $p, q$ : row and column permutation vectors of  $A$  after preprocessing, respectively  
 $n_1$ : the dimension of the current leading block (i.e.,  $B = \hat{A}_{p_{1:n_1}, q_{1:n_1}}$ )  
 $\text{params}$ :  $\alpha_L, \alpha_U, \kappa, \kappa_D, \tau_L, \tau_U$  (adapted for present level),  $\text{max\_steps}$  (for rook pivoting)  
 $\text{level}$ : current level  
 $\text{ibrp}$ : Boolean tag for enabling inverse-based rook pivoting  
 $\text{nr}, \text{nc}$ : number of nonzeros per row and column entry of the original user input matrix, respectively

**outputs:**

$L_B, d_B, U_B$ : approximate  $LDU$  factors of the leading block  
 $L_E, U_F$ : off-diagonal blocks of (11)  
 $p, q$ : updated row and column permutation vectors, respectively  
 $n_1$ : updated leading block dimension

```

1:  $L \leftarrow [1]; U \leftarrow [1]; d \leftarrow []$ 
2: for  $k = 1$  to  $n_1$  do
3:   if  $\text{ibrp}$  then
4:      $p, L, d, U, q \leftarrow \text{ib\_rook\_pivot}(\hat{A}, k, p, L, d, U, q, \kappa, n_1, \text{max\_steps})$  {perform inverse-based root pivoting,
       typically only if level > 1}
5:   else
6:      $d_k \leftarrow a_{p_k q_k} - \ell_{k,1:k-1} D_{1:k-1,1:k-1} u_{1:k-1,k}$  {fan-in update of diagonal entry}
7:   end if
8:    $\tilde{\kappa}_L \leftarrow \|L_{1:k,1:k}^{-1}\|_\infty; \tilde{\kappa}_U \leftarrow \|U_{1:k,1:k}^{-1}\|_1$  {estimate inverse norms of current  $L$  and  $U$  factors}
9:   while  $\kappa_D |d_k| < 1$  or  $\max\{\tilde{\kappa}_L, \tilde{\kappa}_U\} > \kappa$  do
10:    permute entries  $\ell_{k,1:k-1}, d_k$  and  $u_{1:k-1,k}$  to the end; update  $p$  and  $q$  accordingly
11:    break if  $k == n_1$ 
12:     $\tilde{\kappa}_L \leftarrow \|L_{1:k,1:k}^{-1}\|_\infty; \tilde{\kappa}_U \leftarrow \|U_{1:k,1:k}^{-1}\|_1$  {update inverse norms}
13:     $d_k \leftarrow a_{p_k q_k} - \ell_{k,1:k-1} D_{1:k-1,1:k-1} u_{1:k-1,k}$  {recompute diagonal entry due to pivoting}
14:     $n_1 \leftarrow n_1 - 1$  {decrease leading block for factorization}
15:  end while
16:   $\ell_{k+1:n,k} \leftarrow \frac{1}{d_k} (\hat{a}_{p_{k+1:n}, q_k} - L_{k+1:n,1:k-1} D_{1:k-1,1:k-1} u_{1:k-1,k})$  {fan-in update  $k$ th column in  $L$ }
17:   $u_{k,k+1:n} \leftarrow \frac{1}{d_k} (\hat{a}_{p_k, q_{k+1:n}} - \ell_{k,1:k-1} D_{1:k-1,1:k-1} U_{1:k-1,k+1:n})$  {fan-in update  $k$ th row in  $U$ }
18:  select largest  $\lceil \alpha_L \text{nc}_{q_k} \rceil$  and  $\lceil \alpha_U \text{nr}_{p_k} \rceil$  entries in  $\ell_{k+1:n,k}$  and  $u_{k,k+1:n}$ , respectively {scalability-oriented dropping}
19:  drop entries  $\{\ell_{ik} \in \ell_{k+1:n,k} \mid \kappa_D \tilde{\kappa}_L |\ell_{ik}| \leq \tau_L\}$  and  $\{u_{kj} \in u_{k,k+1:n} \mid \kappa_D \tilde{\kappa}_U |u_{kj}| \leq \tau_U\}$  {inverse-based dropping}
20: end for
21:  $L_B \leftarrow L_{1:n_1,1:n_1}; d_B \leftarrow d_{1:n_1}; U_B \leftarrow U_{1:n_1,1:n_1}; L_E \leftarrow L_{n_1+1:n,1:n_1}; U_F \leftarrow U_{1:n_1,n_1+1:n}$ 
22: return  $L_B, d_B, U_B, L_E, U_F, p, q, n_1$ 

```

---

the original (i.e., the top level instead of the present level) input matrix, respectively; see line 18. This dropping strategy plays an important role for HILUCSI and HIF to achieve (near) linear complexity in both space and time. Besides this symbolic dropping, HILUCSI and HIF also adopted an inverse-based dropping [16], which drops every entry  $\ell_{ik}$  such that  $\kappa_D \|L_{1:k,1:k}^{-1}\|_\infty |\ell_{ik}| \leq \tau_L$ , where  $\kappa_D$  and  $\tau_L$  are user-specified thresholds for the upper bound of  $\|D_{1:k,1:k}^{-1}\|$  and the drop tolerance, respectively (see Section 5.2). The dropping for  $U$  is similar; see line 19.

Another core component in `ilu_factorize` is the inverse-based dynamic deferring. In particular, during the fan-in ILU, we dynamically defer  $\ell_{k,1:k-1}$  and  $u_{1:k-1,k}$  (line 10) if we encounter small  $|d_k|$  or large  $\|L_{1:k,1:k}^{-1}\|_\infty$  and  $\|U_{1:k,1:k}^{-1}\|_1$

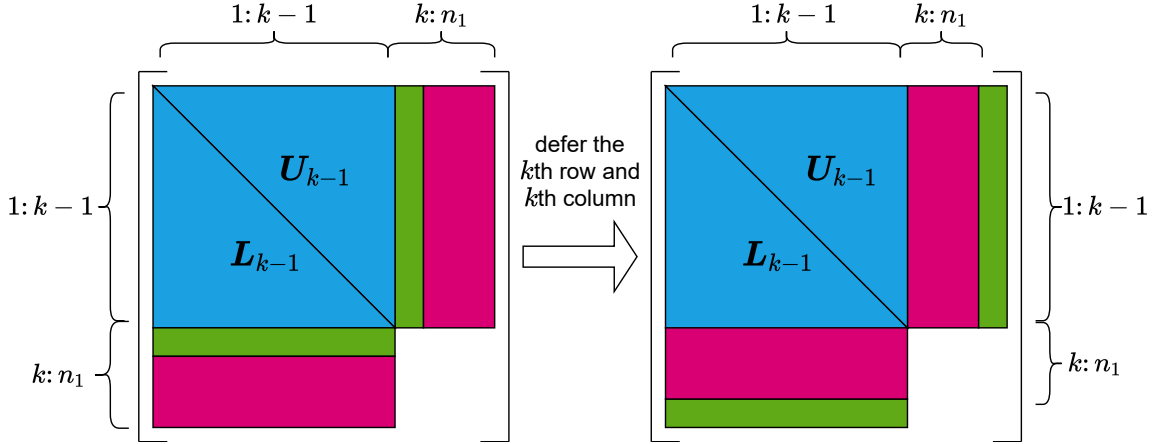


Fig. 2. Illustration of dynamic deferring.  $L_{k-1}$  and  $U_{k-1}$  are shorthand for  $L_{1:k-1,1:k-1}$  and  $U_{1:k-1,1:k-1}$ , respectively. When encountering ill-conditioned factors ( $|d_k| < 1/\kappa_D$  or  $\max\{\|L_{1:k-1,1:k-1}^{-1}\|_\infty, \|U_{1:k-1,1:k-1}^{-1}\|_1\} > \kappa$ ) due to  $\ell_{k,1:k-1}$  or  $u_{1:k-1,k}$  (green regions in left panel), we dynamically defer both  $\ell_{k,1:k-1}$  and  $u_{1:k-1,k}$  to next level (right panel).

(line 9). Figure 2 illustrates the process of dynamic deferring. This deferring is similar to that in [15, 16]; in Section 3.2, we will extend it to support rook pivoting. Note that the inverse-based dropping in line 19 can be replaced by a different dropping strategy, such as that in [59], but we utilized the inverse-based dropping since we are already estimating the inverse norms for deferring.

We note some implementation details. First, in line 18, we use quickselect [44], which has expected linear time complexity. Second, since we need to access both rows and columns of  $\hat{A}$  while computing the fan-in updates (lines 16 and 17), we need to store  $\hat{A}$  (or more precisely,  $A$ ) in both row and column majors. We will describe the data structures in Section 3.5 and Appendix A. Third, the output  $L_E$  and  $U_F$  will only be used to compute the Schur complement in Section 3.3. Afterwards,  $L_E$  and  $U_F$  are discarded, since they can be reconstructed from  $\tilde{E} = \hat{A}_{p_{n_1+1:n}, q_{1:n_1}}$  and  $\tilde{F} = \hat{A}_{p_{1:n_1}, q_{n_1+1:n}}$ , respectively as in (11).

### 3.2 Inverse-based rook pivoting for coarse levels

Dynamic deferring symmetrically permutes rows and columns. Such a permutation strategy works well for reasonably well-conditioned matrices. However, we observe that symmetric permutations alone sometimes lead to relatively large Schur complements for highly ill-conditioned unsymmetric systems. To overcome this issue, we introduce an *inverse-based rook pivoting (IBRP)* for the fan-in ILU, by adapting the rook pivoting [66] for complete LU factorization.

In the standard rook pivoting [66], a pivot is found by searching in the row and column in alternating order until its magnitude is no smaller than those of all other entries in the row and column within the Schur complement. This strategy has a comparable cost as partial pivoting for dense matrices but enables superior stability. However, in the context of fan-in ILU, only the  $k$ th row and column of the Schur complement  $S$  are updated at the  $k$ th step; the remaining part of the Schur complement is not available. Hence, we must modify the pivoting procedure to interleave the search with dynamic permutation and “just-in-time” fan-in updates. Figure 3 illustrates one step of the IBRP. Note that this permutation is more general than the dynamic deferring in Figure 2, in that it can exchange  $\ell_{k,1:k-1}$  with a row in the middle of  $L_{k+1:n_1,1:k-1}$ , and similarly for the rows in  $U$ . Furthermore, the row and column interchanges are not

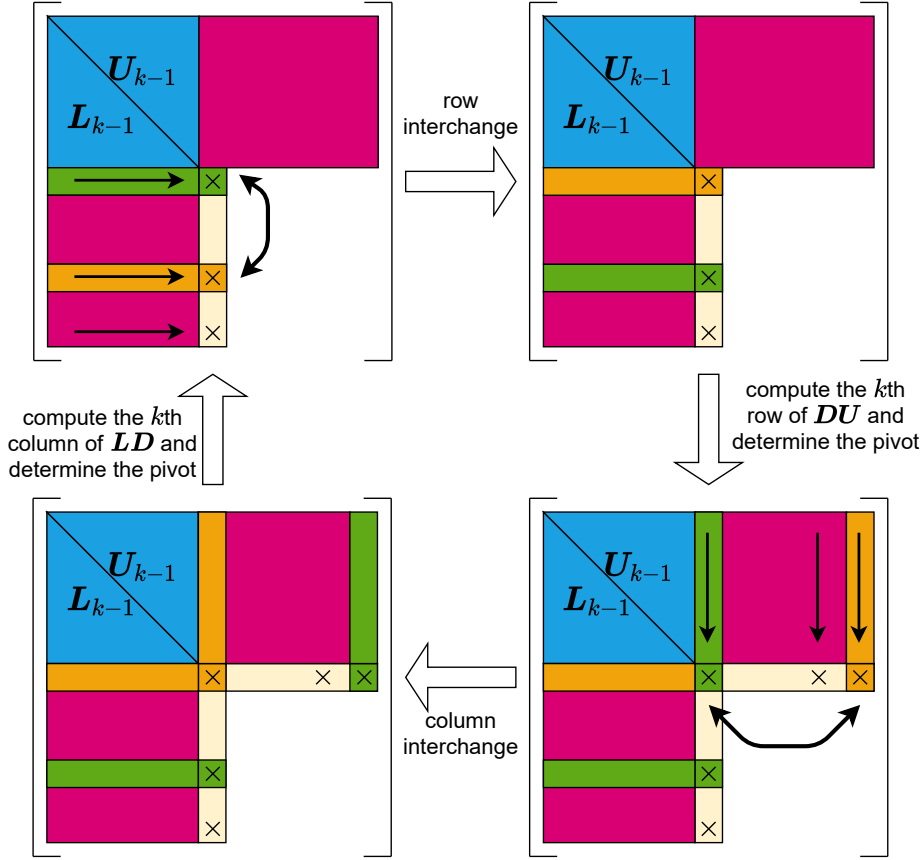


Fig. 3. Illustration of inverse-based rook pivoting in HIF. At the upper-left panel, we update  $d_k$  and nonzeros in  $\ell_{k+1:n,k}$ , find a pivot, and then interchange  $\ell_{k,1:k-1}$  with the pivot row (indicated by curved arrow). The lower-left panel shows the process for  $U$ .

symmetric in general. Note that IBRP requires a more sophisticated data structure to support the row and column interchanges, which we will address in Section 3.5.

Besides the difference dictated by the fan-in update, there are two other significant differences between IBRP and the standard rook pivoting. First, we do not simply use the magnitude to determine the pivot, since it may conflict with dynamic deferring. Instead, we add an inverse-based constraint when searching the pivot, so that the pivot row in  $L$  and pivot column in  $U$  would not arbitrarily enlarge the condition numbers of the  $L$  and  $U$ , respectively. Second, we do not locate the optimal rook pivot whose magnitude is the largest among its row and column; instead, we impose a maximum number of steps of IBRP, controlled by the parameter `max_steps`. For completeness, Algorithm 2 details the inverse-based rook pivoting. Note that we do not scale  $\hat{\ell}$  and  $\hat{u}$  by  $1/d_k$  in lines 2 and 9 in Algorithm 2, compared to  $\ell_{k:n,k}$  and  $u_{k,k:n}$  in lines 16 and 17 in Algorithm 1. This omission of scaling is for efficiency purposes, because the choice of pivot does not depend on the scaling of the entries.

We note an important practical issue. The IBRP can result in significantly denser  $L$  and  $U$  factors because the pivoting may undo the effects of the fill-reduction reordering in the preprocessing step. Hence, we enable IBRP only on the coarser levels (typically for level  $> 1$ ) when dynamic deferring is found to be ineffective. At the coarser levels, we

---

**Algorithm 2** `ib_rook_pivot`( $\hat{A}, k, p, L, d, U, q, \kappa, n_1, \text{max\_steps}$ )

---

**inputs:**

$\hat{A}$ : input scaled matrix (i.e.,  $\hat{A} = WAV$ , passed in as  $A, W$ , and  $V$  separately)  
 $k$ : step count in ILU factorization  
 $p, q$ : row and column permutation vectors of  $A$ , respectively  
 $L, U$ :  $L$  and  $U$  factors at step  $k$ , i.e.  $L_B \cup L_E$  and  $U_B \cup U_F$ , respectively  
 $d$ : diagonal entries at step  $k$   
 $\kappa$ : inverse-norm threshold  
 $n_1$ : leading block dimension  
 $\text{max\_steps}$ : maximum number of rook pivoting steps

**outputs:**

$p, q$ : updated row and column permutation vectors, respectively  
 $L, U$ : updated  $L$  and  $U$  factors, respectively  
 $d$ : diagonal entries with updated  $d_k$

```

1: for  $i = 1$  to  $\text{max\_steps}$  do
2:    $\hat{\ell}_{k:n} \leftarrow \hat{A}_{p_{k:n}, q_k} - L_{k:n, 1:k-1} D_{1:k-1, 1:k-1} u_{1:k-1, k}$  {fan-in update of  $d_k$  and  $\ell_{k+1:n, k}$  without scaling by diagonal}
3:    $r \leftarrow \arg \max \left\{ |\hat{\ell}_r| \mid k+1 \leq r \leq n_1 \text{ and } \left\| \begin{bmatrix} L_{1:k-1, 1:k-1} & 0 \\ L_{r, 1:k-1} & \ell_{r, k} \end{bmatrix}^{-1} \right\|_{\infty} \leq \kappa \right\}$  {find pivot in  $\hat{\ell}_{k+1:n}$ }
4:   if  $r \neq \emptyset$  and  $|\hat{\ell}_k| < |\hat{\ell}_r|$  then
5:      $\ell_{k, 1:k-1} \leftrightarrow \ell_{r, 1:k-1}; p_k \leftrightarrow p_r; \hat{\ell}_k \leftrightarrow \hat{\ell}_r$  {perform row interchange}
6:   else if  $i > 1$  then
7:      $d_k \leftarrow \hat{\ell}_k$ ; break {extract  $d_k$  from  $\hat{\ell}_{k:n}$ }
8:   end if
9:    $\hat{u}_{k:n} \leftarrow \hat{A}_{p_k, q_{k:n}} - \ell_{k, 1:k-1} D_{1:k-1, 1:k-1} U_{1:k-1, k:n}$  {fan-in update of  $d_k$  and  $u_{k, k+1:n}$  without scaling by diagonal}
10:   $c \leftarrow \arg \max \left\{ |\hat{u}_c| \mid k+1 \leq c \leq n_1 \text{ and } \left\| \begin{bmatrix} U_{1:k-1, 1:k-1} & U_{1:k-1, c} \\ 0 & u_{k, c} \end{bmatrix}^{-1} \right\|_1 \leq \kappa \right\}$  {find pivot in  $\hat{u}_{k+1:n}$ }
11:  if  $c \neq \emptyset$  and  $|\hat{u}_k| < |\hat{u}_c|$  then
12:     $u_{1:k-1, k} \leftrightarrow u_{1:k-1, c}; q_k \leftrightarrow q_c; \hat{u}_k \leftrightarrow \hat{u}_r$  {perform column interchange}
13:  else
14:     $d_k \leftarrow \hat{u}_k$ ; break {extract  $d_k$  from  $\hat{u}_{k:n}$ }
15:  end if
16: end for
17: return  $p, L, d, U, q$ 

```

---

also enlarge the scalability-oriented fill factors  $\alpha_L$  and  $\alpha_U$  to preserve more *fills* introduced by IBRP. Our experiments show that applying IBRP on coarser levels can significantly reduce the size of the final Schur complement for some challenging problems, as demonstrated by the example in Table 1.

### 3.3 Computing and factorizing Schur complements

After finishing `ilu_factorize`, we need to compute the Schur complement  $S$  based on (12). This step involves a sparse matrix-matrix (SpMM) multiplication, for which we adopt the algorithm as described in [6]. The space and time complexity of SpMM depends on the nonzeros in  $L_E$  and  $U_F$ . To achieve near-linear complexity, we apply scalability-oriented dropping *before* SpMM to the rows and columns of  $L_E$  and  $U_F$ , respectively. Recall that in `ilu_factorize` we already applied scalability-oriented dropping to the columns and rows of  $L_E$  and  $U_F$ , respectively. Hence, the nonzeros both rows and columns in  $L_E$  and in  $U_F$  are well controlled, allowing us to effectively bound the complexity of  $S$ . In

Table 1. Effectiveness of IBRP for reducing the final Schur complement size for the testing matrix shyy161 from the SuiteSparse Matrix Collection [23].  $\dim(\mathcal{N})$  indicates the dimension of the null space, and  $S_m$  denotes the final Schur complement in HIF. We factorized the testing matrix using HIF with and without IBRP, and we report the factorization time (factor time) and nnz ratio (i.e.,  $\text{nnz}(M)/\text{nnz}(A)$ , aka fill ratio in [57]). We solved the consistent system with right-hand side  $\mathbf{b} = A\mathbf{1}$  (where  $\mathbf{1} = [1, 1, \dots, 1]^T$ ) using GMRES(30) with relative residual tolerance  $10^{-6}$ . The computing environment for running the test can be found in Section 6. Timing results for GMRES were negligible thus omitted.

$n$	nnz	$\dim(\mathcal{N}(A))$	w/ IBRP	$S_m$ in HIF		fac. time	#levels	nnz ratio	GMRES iter.
				$n$	$\dim(\mathcal{N}(S_m))$				
76,480	329,762	$\geq 50$	yes	1,407	50	2.51	5	12.0	15
			no	9,394	48	226	2	304	2

---

**Algorithm 3** `rrqr_final_schur`( $S, \kappa_{\text{rrqr}}$ )

---

**inputs:**
 $S$ : final Schur complement of size  $n_s \times n_s$ 
 $\kappa_{\text{rrqr}}$ : condition number threshold for determining numerical rank (default value is  $\epsilon_{\text{mach}}^{-2/3}$ )

**outputs:**
 $Q, R$ :  $Q$  and  $R$  factors of  $S$ 
 $p$ : permutation vector in QRCP

 $r$ : numerical rank of  $S$ 

- 1: factorize  $S = QRP^T$  {compute QRCP via xGEQP3}
  - 2: **for**  $r = 1$  **to**  $n_S$  **do**
  - 3:   update estimated  $\|R_{1:r,1:r}\|_2$  and  $\|R_{1:r,1:r}^{-1}\|_2$  {incremental condition number estimation via xLAIC1}
  - 4:   **if**  $\|R_{1:r,1:r}\|_2 \|R_{1:r,1:r}^{-1}\|_2 < \kappa_{\text{rrqr}}$  **then**
  - 5:      $r \leftarrow r + 1$
  - 6:   **break**
  - 7:   **end if**
  - 8: **end for**
  - 9: **return**  $Q, R, p, r$
- 

contrast, if we applied dropping *after* SpMM, the complexity of SpMM may be higher. Note that after computing  $S$ , we drop both  $L_E$  and  $U_F$  as they can be reconstructed from the other terms as in (11), and then factorize  $S$  recursively.

In HIF, the final Schur complement is factorized by rank-revealing QR (or truncated QRCP) in order to guarantee the stability of the preconditioner. Algorithm 3 outlines the procedure. We note a couple of details in the algorithm. First, line 1 computes QRCP  $SP = QR$  for  $S \in \mathbb{R}^{n_S \times n_S}$ , where  $P$  is a permutation matrix, and  $r_{11} \geq r_{22} \geq \dots \geq r_{n_S n_S} \geq 0$ . The QRCP has a time complexity of  $\mathcal{O}(n_S^3)$ . Second, lines 2–8 determine the numerical rank of  $S$  by comparing the estimated condition number against a threshold  $\kappa_{\text{rrqr}}$ , which defaults to  $\kappa_{\text{rrqr}} = \epsilon_{\text{mach}}^{-2/3}$ . We estimate the 2-norm condition number using the incremental estimator in [13], which has a linear complexity per step. Hence, the overall computational cost is dominated by QRCP. For efficiency, we implement the QRCP and condition-number estimator using LAPACK kernel functions xGEQP3 and xLAIC1, respectively.

Due to the cubic time complexity of QRCP, we would like to make  $n_S$  as small as possible, and ideally have  $n_S = \mathcal{O}(\sqrt[3]{n})$ , where  $n$  is the number of unknowns in the original system. This high complexity was the motivation to use IBRP within multilevel ILU. In addition, we would also like to prevent having too many low-quality ILU levels. As a tradeoff, we trigger QRCP based on the following criteria. In `ilu_factorize`, let  $n_0$  be the initial leading block dimension

after preprocessing, i.e., the input  $n_1$  in Algorithm 1, and let  $d$  be the total number of dynamic deferrals. If more than 75% entries are dynamically deferred during fan-in update, i.e.,  $d/n_0 \geq 0.75$ , then we discard incomplete factorization in that level and use RRQR on its input. In addition, if more than 60% entries are dynamically deferred, i.e.,  $d/n_0 \geq 0.6$ , then we apply RRQR on the remainder Schur complement.

### 3.4 Preprocessing with static deferring

In Figure 1, an important step was the preprocessing at each step, which computes a block structure  $\begin{bmatrix} \hat{B} & \hat{F} \\ \hat{E} & \hat{C} \end{bmatrix}$ . The preprocessing in HIF performs equilibration, static deferring, and fill-reduction reordering, in that order. Equilibration improves stability by computing  $P^T W A V Q = \tilde{A}$ , where  $W$  and  $V$  correspond to row and column scaling matrices, and  $P$  and  $Q$  correspond to row and column permutation matrices. We utilize MC64 [26], which computes unsymmetric equilibration, for which  $Q = I$ . For (nearly) pattern symmetric levels, we symmetrize the output of MC64 by setting  $W = V = \sqrt{WV}$  and  $Q = P$  as in [53]. Note that for structurally singular systems, MC64 sometimes yields unstable scaling factors that may be arbitrarily large or small [48]. The symmetrization process overcomes the issue; for unsymmetric equilibration, we also symmetrize the scaling factors by setting  $w_i = v_i = \sqrt{w_i v_i}$  if  $\max\{w_i, v_i\} / \min\{w_i, v_i\} > \beta$ , where  $\beta$  is 1000 by default. After symmetric equilibration, we permute a row and its corresponding column to the lower-right corner if its diagonal entry is nearly zero. We refer to this process as *static deferring*, which naturally yields a block structure  $\begin{bmatrix} B & F \\ E & \hat{C} \end{bmatrix}$ . Afterwards, we apply fill-reduction reordering on  $B$  and then permute  $E$  and  $F$  correspondingly, which leads to the final block structure  $\begin{bmatrix} \hat{B} & \hat{F} \\ \hat{E} & \hat{C} \end{bmatrix}$ . We use RCM [31] and AMD [2] for symmetric and unsymmetric reordering, respectively, because RCM is more efficient and has been shown to work better for symmetric ILU [10, 38].

### 3.5 Efficient data structures and complexity analysis

To implement HIF efficiently, we must perform all its core operations in linear time with respect to the number of nonzeros. In particular, the fan-in updates of  $\ell_{k+1:n,k}$  and  $u_{k+1:n,k}$  at  $k$ th `ilu_factorize` (cf. lines 16 and 17 in Algorithm 1 and lines 2 and 9 in Algorithm 2) requires efficient sequential access of  $L$  and  $U$  in both rows and columns. More importantly, the deferring and pivoting operations require interchanging rows and columns in  $L$  and  $U$  dynamically. Although the data structure in [55] supports fan-in updates efficiently, it does not support deferring or rook pivoting. Under these considerations, we developed flexible, three-tiered data structures, which extended the data structure in [55] to support deferring and pivoting, as we describe in Appendix A. This three-tiered data structure augments the standard compressed sparse column or row (aka CSC and CSR) formats either partially or fully. We use the partially augmented version when rook pivoting is disabled, especially at the top levels, since it has a smaller memory footprint; the fully augmented version is used when rook pivoting is enabled, which in general occurs only at coarser levels.

Assuming the number of nonzeros per row and column in the input mesh is bounded by a constant, which is typically the case for linear systems arising from partial differential equations, the augmented data structures enable all the core components in HIF to be performed in linear time at each level. We outline the analysis as follows. First, the fan-in update can be performed in linear time proportional to the number of nonzeros, thanks to the use of augmented data structure [55]. Second, the incremental update of  $\|L_{1:k,1:k}^{-1}\|_\infty$  and  $\|U_{1:k,1:k}^{-1}\|_1$  also costs linear time with respect to the number of nonzeros in  $L$  and  $U$ , respectively (see e.g., [34]). Third, the partially augmented data structures allow the



permutations in deferring can be performed in linear time complexity, as shown in [20]. Fourth, the fully augmented data structures allow each row interchange in rook pivoting to be performed in time proportional to the number of nonzeros, assuming the number of nonzeros in each row is a constant. This step is the most complicated, and we defer its analysis to Appendix B. Fifth, the time complexity of SpMM in Section 3.3 is proportional to the number of nonzeros in the product. Since the scalability-oriented dropping ensures that each row and column of  $L_E$  and  $U_F$  is bounded by a constant  $C$ , so the number of nonzeros per row and per column in the product  $L_E D_B U_F$  is bounded by  $C^2$ . Finally, assuming the number of rows in the final Schur complement is bounded by  $O(n^{1/3})$ , we conclude that HIF guarantees linear time complexity per level (excluding its preprocessing steps) under the assumptions as mentioned above.

Note that HIF does not guarantee that the number of levels is bounded by a constant. Furthermore, the time complexity of AMD reordering is quadratic in the worst-case case [41]. Hence, the total time complexity of HIF may not be linear. Nevertheless, the number of levels is typically a small constant, and the computational cost of AMD is typically negligible. Hence, we do observe linear asymptotic growth for the overall HIF across all levels empirically.

#### 4 MULTILEVEL TRIANGULAR SOLVES AND MATRIX-VECTOR MULTIPLICATIONS

To use the HIF as a preconditioner, we typically need a procedure similar to triangular solves. We shall refer to it as a *multilevel triangular solver*. As an illustration, let  $\mathbf{y} = \begin{bmatrix} \mathbf{y}_1 \\ \mathbf{y}_2 \end{bmatrix}$  be a block vector corresponding to  $\tilde{\mathbf{B}}$  and  $\mathbf{C}$  in the two-level ILU  $\mathbf{M}$  in (11). In this case,  $\mathbf{W}^{-1} \mathbf{P} \mathbf{M} \mathbf{Q}^T \mathbf{V}^{-1}$  is a preconditioner of  $\mathbf{A}$ . The multilevel solver computes

$$\mathbf{M}^g \mathbf{y} = \begin{bmatrix} \tilde{\mathbf{B}}^{-1} \mathbf{y}_1 \\ 0 \end{bmatrix} + \begin{bmatrix} -\tilde{\mathbf{B}}^{-1} \mathbf{F} \\ \mathbf{I} \end{bmatrix} \mathbf{S}^g (\mathbf{y}_2 - \mathbf{E} \tilde{\mathbf{B}}^{-1} \mathbf{y}_1). \quad (19)$$

We further compute  $\mathbf{S}^g \mathbf{y}_1$  recursively, which leads to the multilevel solver. Algorithm 4 details this recursive procedure. Note that Algorithm 4 also supports the use of  $\mathbf{M}^H$  to construct a preconditioner for  $\mathbf{A}^H$  based on (15).

When solving inconsistent systems, such as the computation of the null-space vector, using  $\mathbf{G} = \tilde{\mathbf{M}}^g$  as the preconditioning operator may be insufficient. In this setting, it is desirable to enable iterative refinement with HIF to construct a variable preconditioner for FGMRES, as described in [48]. Specifically, given equation  $\mathbf{A} \mathbf{v} = \mathbf{q}$ , HIFIR iteratively computes

$$\mathbf{v}_j = (\mathbf{I} - \mathbf{M}^g \mathbf{A}) \mathbf{v}_{j-1} + \mathbf{M}^g \mathbf{q} = \mathbf{v}_{j-1} - \mathbf{M}^g \mathbf{r}_{j-1} \quad (20)$$

for  $j = 1, 2, \dots$ , where  $\mathbf{r}_{j-1} = \mathbf{q} - \mathbf{A} \mathbf{v}_{j-1}$  is the residual vector with  $\mathbf{v}_0 = 0$ , and  $\mathbf{M}^g \mathbf{r}_{j-1}$  is computed by Algorithm 4. Note that when computing null-space vectors, the condition number of  $\mathbf{R}_1$  in the RRQR of  $\mathbf{S}_m$  can be as large as  $1/\epsilon_{\text{mach}}$ , so it would have a different numerical rank of  $\mathbf{S}_m$  compared to that when solving consistent systems as described in Section 3.3. For this reason, Algorithm 4 has a parameter  $r$  to allow the user passing in different numerical ranks of  $\mathbf{S}_m$ . When choosing the number of iterations in the iterative refinement, HIFIR terminates the iteration after a maximum number of iterations. We increase this upper bound on the iterations at every restart for FGMRES. We refer readers to [48] for the analysis of this adaptive procedure.

Besides multilevel triangular solves, HIF also supports the computation of the multiplication  $\tilde{\mathbf{M}}$  with a vector. As an illustration, given  $\mathbf{x} = \begin{bmatrix} \mathbf{x}_1 \\ \mathbf{x}_2 \end{bmatrix}$  in a two-level factorization, the multiplication can be written as

$$\tilde{\mathbf{M}} \mathbf{x} = \begin{bmatrix} \tilde{\mathbf{B}} \\ \mathbf{E} \end{bmatrix} \mathbf{x}_1 + \begin{bmatrix} \mathbf{I} \\ \mathbf{E} \tilde{\mathbf{B}}^{-1} \end{bmatrix} \mathbf{F} \mathbf{x}_2 + \begin{bmatrix} 0 \\ \mathbf{S} \mathbf{x}_2 \end{bmatrix}. \quad (21)$$

**Algorithm 4** `hif_solve`( $M, y, r, \text{trans}, \text{level} = 1$ )**inputs:**

$M$ : a structure containing HIF preconditioner  $M$   
 $y$ : right-hand side vector  
 $r$ : numerical rank used in the final RRQR factorization  
 $\text{trans}$ : Boolean flag indicating whether to solve  $M^{gH}y$   
 $\text{level}$ : level counter in the HIF preconditioner (default to 1 at top level)

**output:**

$x$ : solution vector  $M^g y$  or  $M^{gH} y$

```

1: extract  $n_1, n, L_B, D_B, U_B, E, F, P, Q, W$ , and  $V$  for current level from  $M$ 
2: if  $\text{trans}$  then
3:    $L_B, U_B \leftarrow U_B^H, L_B^H, D_B \leftarrow \bar{D}_B$  {construct conjugate transpose}
4:    $E, F \leftarrow F^H, E^H$ 
5:    $W \leftrightarrow V; P \leftrightarrow Q$ 
6: end if
7:  $y \leftarrow P^T W y$  {scale and permute right-hand side}
8:  $x_{1:n_1} \leftarrow U_B^{-1} D_B^{-1} L_B^{-1} y_{1:n_1}$ 
9:  $x_{n_1+1:n} \leftarrow y_{n_1+1:n} - E x_{1:n_1}$ 
10: if final level then
11:   extract  $\hat{Q}, \hat{R}$ , and  $\hat{P}$  of QRCP of  $S_m$  (or of  $S_m^H$  if  $\text{trans}$ ) from  $M$ 
12:    $x_{n_1+1:n} \leftarrow \hat{P}_{:,1:r} \hat{R}_r^{-1} \hat{Q}_{:,1:r}^H x_{n_1+1:n}$  {solve on final Schur complement with numerical rank  $r$ }
13: else
14:    $x_{n_1+1:n} \leftarrow \text{hif\_solve}(M, x_{n_1+1:n}, r, \text{tran}, \text{level} + 1)$ 
15: end if
16:  $x_{1:n_1} \leftarrow y_{1:n_1} - F x_{n_1+1:n}$ 
17:  $x_{1:n_1} \leftarrow U_B^{-1} D_B^{-1} L_B^{-1} x_{1:n_1}$ 
18: return  $V Q x$  {scale and permute  $x$ }
```

The multiplication of  $x_2$  by the Schur complement, i.e.  $Sx_2$ , is then computed recursively, leading to the multilevel matrix-vector multiplication. The control flow of this recursive algorithm is similar to that of Algorithm 4, and it is helpful when we need  $\tilde{M}$  as an approximation of  $A$  (instead of using  $\tilde{M}^g$  as an approximation to  $A^g$ ). In addition, it is also useful for some advanced preconditioners for singular systems, which we will report in the future.

## 5 SOFTWARE DESIGN AND USER INTERFACES

In this section, we describe our software design and the user interfaces of HIFIR, including its C++ programming interface as well as the high-level interfaces for Python and MATLAB. We refer the readers to the official documentation <https://hifirworks.github.io/hifir/> for more detailed documentation of HIFIR.

### 5.1 Design considerations

When designing HIFIR, we have focused on three key factors: efficiency, flexibility, and ease-of-integration into other codes. Under these considerations, we chose to implement the core components of HIFIR in C++-11 using C++ templates in a header-only fashion while providing high-level interfaces in Python and MATLAB. C++ is a powerful programming language for scientific computing and is highly efficient. For efficient kernel computations, we link HIFIR with LAPACK and we ease the linking by leveraging compiler directives and macros. In terms of flexibility, HIFIR supports different data types, such as float, double, and `std::complex<double>`, through C++ templates. In addition, mixed data types are

```

struct hif::Params {
    double alpha_L;           // scalability oriented threshold for L (10)
    double alpha_U;           // scalability oriented threshold for U (10)
    double kappa;             // inverse norm threshold for L and U (3)
    double kappa_d;           // inverse norm threshold for D (3)
    double tau_L;             // drop tolerance for L (0.0001)
    double tau_U;             // drop tolerance for U (0.0001)
    double beta;              // safeguard for scaling in equilibration (1000)
    double kappa_rrqr;        // conditioning threshold for RRQR (eps ^ (-2/3))
};

```

Fig. 4. Core control parameters in HIFIR library along with default values in parentheses.

supported, for example, to compute the factorization in double precision while exporting it in single precision during the solve step. In addition, the use of C++ also makes it easier to integrate with other linear-algebra packages (such as Eigen [36], Blaze [46], SuperLU [56], PETSc [5], etc.) and scientific-computing packages (such as Trilinos [42]). The use of C++ in HIFIR eases its integration with such libraries. The header-only design of HIFIR is similar to that of Eigen [36]. This design significantly simplifies the installation and build process in that the user only needs to include the header file `hifir.hpp` and link with LAPACK libraries. For ease of prototyping, we also provide high-level interfaces in Python and MATLAB through `hifir4py` and `hifir4m`, respectively; see Section 5.4.

## 5.2 Control parameters

The algorithm described in Section 3 involved several control parameters, as we summarize some key parameters in Figure 4 as a C++ structure. The first six parameters correspond to  $\alpha_L$ ,  $\alpha_U$ ,  $\kappa$ ,  $\kappa_D$ ,  $\tau_L$ , and  $\tau_U$  for the top level in Algorithm 1; note that HIF automatically adapt these parameters for coarser levels. Their default values were obtained based on the experiments in [20]. The seventh and eighth parameters in Figure 4 corresponds to  $\beta$  described in Section 3.4 and  $\kappa_{rrqr}$  in Algorithm 3, respectively. We omit some additional parameters for simplicity.

The default values typically work well for PDE-based systems. They are appropriate for both double- and single-precision computations, since the thresholds are far greater than their corresponding machine epsilons. We present some guidelines in tuning the first six parameters, based on theoretical analysis and extensive experimentation:

- **alpha\_L, alpha\_U:** These control the scalability-oriented dropping, and they are critical in achieving linear-time complexity of HIFIR at each level. The recommended values are between 2 and 20. While the default values  $\alpha_L = \alpha_U = 10$  are robust, the user may reduce them to  $\alpha_L = \alpha_U = 3$  for PDE-based systems (including saddle-point problems) for better efficiency;
- **kappa, kappa\_d:** These control the inverse norms of the triangular factors ( $L$  and  $U$ ) and diagonal factor ( $D$ ), respectively. Their recommended range is between 3 and 5. The default values  $\kappa = \kappa_D = 3$  are robust, but the user may increase them to  $\kappa = \kappa_D = 5$  for PDE-based systems for better efficiency;
- **tau\_L, tau\_U:** These control numerical droppings and they are secondary compared to  $\alpha_L$  and  $\alpha_U$ . The default values  $\tau_L = \tau_U = 10^{-4}$  are robust; one may increase them to  $\tau_L = \tau_U = 10^{-2}$  for PDE-based systems for better efficiency. One could even set them to zero without losing (near) linear time complexity, as long as  $\alpha_L$  and  $\alpha_U$  are within the recommended ranges. Note that large  $\kappa$  and  $\kappa_D$  may implicitly reduce the drop tolerances.

### 5.3 Programming interfaces in C++

The core components of HIFIR are implemented using generic object-oriented programming with C++-11. All data structures and algorithms in HIFIR are implemented as C++ template classes and functions.

*5.3.1 Basic data types.* HIFIR has two basic data types: sparse matrices and vectors. The sparse matrices in HIF include CSC, CSR, and their partially or fully augmented counterparts as described in Appendix A. We will use CSR as the demonstration in the following. The class of CSR matrix in HIF is `hif::CSR<ValueType, IndexType>`, of which the two template arguments correspond to the value data type (e.g., float, double, `std::complex<double>`, etc.) and the index data type (e.g., int, long, etc.), respectively. For instance, a commonly used type is `hif::CSR<double, int>`. A CSR instance can either wrap or own the data; the former mode allows the user to create a “view” into a CSR matrix owned by another software library, so it is more memory efficient and is preferred. For example, to wrap external data for read-only access by HIF, one can use the helper function

```
template<ValueType , IndexType> const hif::CSR<ValueType , IndexType> hif::
    wrap_const_csr(IndexType nrows , IndexType ncols , const IndexType *
        row_ptr , const IndexType *col_ind , const ValueType *vals);
```

where `row_ptr`, `col_ind`, and `vals` are read-only. HIF also provides an interface to construct a CSR matrix from scratch; we omit the details for simplicity. Note that the augmented CSC and CSR data structures are used internally by HIF, so we omit their interface definitions.

When using HIF as a preconditioner, the right-hand side and solution vectors need to be passed in as arrays. HIF uses a generic interface compatible with STL sequence containers such as `std::vector`. For memory efficiency, HIF also provides a container `hif::Array<ValueType>` for wrapping user-allocated arrays. The user can create mutable and immutable instances by using one of the helper functions:

```
template<ValueType> hif::Array<ValueType> hif::wrap_array(std::size_t n,
    ValueType *vals);
template<ValueType> const hif::Array<ValueType> hif::wrap_const_array(std::
    size_t n, const ValueType *vals);
```

If C++-20 is used, then `std::span<ValueType>` can be used in place of `hif::Array<ValueType>`. Note that `hif::Array` can also own the data; in this case, one can use a construct of `hif::Array` similar to that of `std::vector`.

*5.3.2 Interfaces for HIF preconditioners.* The algorithms for HIF are encapsulated in a class `hif::HIF<ValueType=double, IndexType=int>`, of which the two template arguments are similar to those of `hif::CSR` and specify the data types used by the internal augmented CSC and CSR formats as well as the output format. The class has two main interfaces: factorization and multilevel solve. In the following, we will use `dHIF` as an alias for `hif::HIF<double, int>` as a demonstration.

We first describe the member functions for computing the factorization, which is provided by the template function

```
template<class MatType> void dHIF::factorize(const MatType &A, const hif::
    Params &params=hif::DEFAULT_PARAMS);
```

where `MatType` is typically `hif::CSR<ValueType, IndexType>` or `hif::CSC<ValueType, IndexType>`. However, the interface allows the use of different `ValueType` and `IndexType` for `hif::HIF` and `MatType`. For example, the input may be in double precision, and the preconditioner can be built in single precision. However, if the input matrix is complex, then

ValueType of `hif::HIF` must also be complex and vice versa. The second argument passes in the control parameters as described in Section 5.2, where the default is a static variable in `hif`.

The interface for the multilevel solve is provided by the template function

```
template<class RhsType, class SolType> void dHIF::solve(const RhsType &b,
    SolType &x, bool trans=false, int rnk=0);
```

where `b` and `x` are the right-hand side and the solution vector, respectively. The interfaces for `RhsType` and `SolType` should be compatible with `const hif::Array<ValueType>` and `hif::Array<ValueType>`, respectively, where their `ValueType` may differ from each other and also differ from that of `hif::HIF`. The optional Boolean argument `trans` indicates whether to apply the preconditioner itself or the (conjugate) transpose. The argument `rnk` specifies the rank for the RRQR for the final Schur complement; its default value 0 indicates to use the rank determined by `hif::HIF` from  $\kappa_{\text{rrqr}}$ . The user can set `rnk` to  $-1$  to use a larger rank determined from  $\kappa_{\text{rrqr}} = 1/\epsilon_{\text{mach}}$  for the computation of the null spaces.

Besides the above main interfaces, `hif::HIF` also offers `hif::HIF::hifir` for multilevel solve with iterative refinement and `hif::HIF::mmultiply` for multilevel matrix-vector multiplication. Their interfaces are as follows:

```
template<class MatType, class RhsType, class SolType> void dHIF::hifir(
    const MatType &A, const RhsType &b, SolType &x, int nirs, bool trans=
    false, int rnk=-1);
template<class RhsType, class SolType> void dHIF::mmultiply(const RhsType &
    b, SolType &x, bool trans=false, int rnk=-1);
```

These two functions are more useful for solving singular systems, and hence their default values for `rnk` is  $-1$  instead of 0. The argument `nirs` specifies the number of iterations of iterative refinement.

#### 5.4 High-level interfaces for MATLAB and Python

It is often more productive for prototyping and academic research to use a high-level programming language such as MATLAB, GNU Octave, and Python. For this reason, we have developed `hifir4m` and `hifir4py` to allow the users to access HIFIR from these languages.

For the MATLAB interface, `hifir4m`, which also supports GNU Octave, provides three key functions in its high-level programming interface. The first function constructs a handle to a HIF object for a matrix `A` from either `A` itself or an optional “sparsifier” `S`, with the interface

```
function hif = hifCreate(A [, S, varargin])
```

where `A` and `S` can be MATLAB’s built-in sparse format matrices or MATLAB struct containing the three CSR fields, and `varargin` specifies name-value pairs, such as (`...’, ‘alpha_L’, 5, ‘alpha_U’, 5, ‘mixed’, true`). The matrix `A` and `S` can be single or double precision and can be real or complex. The second function applies the preconditioner, with the interface

```
function y = hifApply(hif, x [, op, rnk, nirs])
```

where the optional argument `op` can be one of ‘S’, ‘SH’, ‘M’, and ‘MH’ for  $M^g x$ ,  $M^{gH} x$ ,  $Mx$ , and  $M^H x$ , respectively, `rnk` specifies the rank for truncated RRQR, and `nirs` specifies the number of iterative refinements for  $M^g x$  and  $M^{gH} x$ . To destroy the HIF object, the user can call

```
delete(hif)
```

manually, or leave it to MATLAB to delete it automatically. In addition, hifir4m offers two high-level drivers, gmresHif and pipitHifir, for solving nonsingular and singular systems, respectively. Their interfaces are similar to MATLAB's build-in gmres.

For the Python interface, hifir4py offers two sets of interfaces: an intermediate-level interface consistent with the C++ version implemented using Cython [7], and a high-level interface consistent with the MATLAB version with support for SciPy sparse matrices [77].

## 6 ILLUSTRATIONS OF HIFIR FOR VARIOUS APPLICATIONS

For HIFIR and its predecessor HILUCSI, we have reported extensive comparisons with some prior state-of-the-art preconditioners [20, 21, 48, 49]: In [20], we compared HILUCSI with supernodal ILUTP in SuperLU [56, 57] and multilevel ILU in ILUPACK [15] for indefinite systems; in [21], we compared HILUCSI with some customized preconditioners (including *pressure convection diffusion (PCD)* [51, 74], *least-squares commutator (LSC)* [28], and modified augmented Lagrangian preconditioner [9, 62]) in Newton-GMRES method for solving the stationary incompressible Navier–Stokes equations; in [49], we compared HILUCSI with ILU(0) [70] and BoomerAMG in hypre [45] as building blocks for several block preconditioners for solving time-dependent advection-diffusion equations with high-order finite element and finite difference methods for spatial discretization and fully implicit multistage Runge–Kutta schemes; in [48], we compared HIFIR with RIF-preconditioned LSMR [12, 30] and implicitly restarted Lanczos bidiagonalization [4] for computing null-space vectors and for solving inconsistent singular systems. In this section, we illustrate HIFIR for some of these applications, using some of the aforementioned state-of-the-art techniques as points of reference. We conducted our tests on a single node of a cluster running CentOS 7.4 with dual 2.5 GHz 12-core Intel Xeon E5-2680v3 processors and 64 GB of RAM. We compiled HIFIR by GCC with optimization options -O3 and -ffast-math. For all the tests, we used right-preconditioned GMRES with restart [70, Section 9.3.2], and the dimension of KSP space is limited to 30, i.e., GMRES(30).

### 6.1 Helmholtz equation

As the first illustration, we solved the Helmholtz equation over  $\Omega = [0, 1]^3$

$$-\Delta u - k^2 u = f \quad (22)$$

with Dirichlet boundary conditions  $u = u_D$  on  $\partial\Omega$ , where  $k > 0$  is the wave number and  $f$  is a source term. Such systems are notoriously difficult to solve for have wave numbers [29]. We discretized the equation using the Galerkin finite element methods (FEM) with quadratic tetrahedral (aka  $P_2$ ) elements, which we implemented using FEniCS v2019.1.0 [1, 58]. We constructed the right-hand side and the boundary conditions using the method of manufactured solutions with the exact solution  $u(x, y, z) = \cos(\pi x) \sin(\pi y) \sin(\pi z)$ . Given a consistent numerical discretization method for (22), we arrive at the following system of equations

$$(K - k^2 M) \mathbf{u}_h = \mathbf{f}_h, \quad (23)$$

where  $K$  and  $M$  are the stiffness and mass matrices, respectively, and  $\mathbf{u}_h$  and  $\mathbf{f}_h$  are vectors containing nodal values of  $u$  and  $f$ , respectively. Note that  $K$  and  $M$  are (symmetric) positive definite, but the coefficient matrix  $K - k^2 M$  can be positive definite, indefinite, or even singular. We chose three different wave numbers,  $k = 1, 5$ , and  $10$ . The first two resulted in positive-definite systems, and the third resulted in indefinite systems.

Table 2. Results for systems arising from the Helmholtz equation discretized by  $P_2$  FEM, solved using GMRES(30) with HIF compared to with supernodal ILUTP in SuperLU and ILUTP in WSMP as the right preconditioner. The condition numbers were estimated using condst function in MATLAB. Times are in seconds. Leaders are in boldface.

mesh	$n$	nnz	$k$	cond.	HIF			supernodal ILUTP			WSMP/ILUTP		
					fac. time	tot. time	iter.	fac. time	tot. time	iter.	fac. time	tot. time	iter.
coarse	132,651	3,195,529	1	8.8e4	3.15	3.46	<b>8</b>	20.2	21.1	11	<b>2.25</b>	<b>2.91</b>	23
			5	6.4e5	3.1	3.47	<b>8</b>	20.9	21.6	12	<b>2.26</b>	<b>3.37</b>	36
			10	6.5e5	3.03	<b>3.81</b>	<b>22</b>	19.8	21.8	25	<b>2.27</b>	5.42	103
medium	357,911	9,070,749	1	2.4e5	8.82	<b>9.62</b>	<b>8</b>	115	117	12	<b>7.85</b>	10.8	30
			5	1.8e6	9.02	<b>9.89</b>	<b>9</b>	117	120	13	<b>7.86</b>	11.9	34
			10	1.8e6	8.9	<b>10.7</b>	<b>16</b>	116	120	24	<b>7.9</b>	25.1	192
fine	1,092,727	28,814,525	1	7.4e5	<b>29.8</b>	<b>33.8</b>	<b>11</b>	903	941	15	35.5	46.1	32
			5	5.4e6	<b>30.1</b>	<b>34.1</b>	<b>11</b>	918	944	16	35.4	47.9	37
			10	5.5e6	<b>29.8</b>	<b>35.5</b>	<b>16</b>	903	954	20	35.1	77.4	141

To assess the effectiveness of HIF, we assembled three systems using meshes with 93,750, 257,250, and 795,906 quadratic elements, respectively. We solved the systems using  $\text{rtol} = 10^{-6}$  GMRES(30) and  $\tau = 10^{-2}$ ,  $\kappa = 5$ , and  $\alpha = 3$  for double-precision HIF. For each of these systems, HIF ended up producing a four-level factorization with nnz ratios (i.e., the number of nonzeros in the preconditioner versus that in the input matrix) of about 2.7. As points of reference, we also solved the systems using GMRES(30) with the supernodal ILUTP in SuperLU v5.2.2 [56, 57] and ILUTP in WSMP v20.12 [37, 39] as the right preconditioners with  $\text{droptol} = 10^{-2}$ . As can be seen from Table 2, HIF was the fastest for seven out of nine cases, and WSMP was the fastest for two small cases. SuperLU was substantially slower than both HIF and WSMP. Nevertheless, SuperLU was relatively insensitive to the wave numbers in terms of factorization and total times, as was HIF. In contrast, WSMP had a significant increase in the solve times for  $k = 10$ , indicating that ILUTP in WSMP is less optimized for indefinite systems than for positive-definite systems. In addition, the computational cost of WSMP increased at a faster rate than HIF as the problem size increased. As a result, HIF was about a factor of 2.2 faster than WSMP for  $k = 10$  on the finest mesh. The better performance of HIF was mostly due to its scalability-oriented dropping. It is worth noting that WSMP supports parallel ILUTP and all of our comparisons were conducted in serial. Parallel ILUTP in WSMP may potentially outperform HIF on a multicore computer, but parallel ILUTP is less robust than serial ILUTP in WSMP and caused GMRES to stagnate for larger systems in our tests.

## 6.2 Linear elasticity with pure traction boundary conditions

In this illustration, we considered the linear-elasticity model of a solid body  $\Omega \subset \mathbb{R}^3$ ,

$$-\nabla \cdot \sigma = f, \quad (24)$$

where  $\sigma$  and  $f$  are Cauchy stress tensor and body force per unit volume, respectively. For isotropic material,  $\sigma = \lambda(\nabla \cdot \mathbf{u})\mathbf{I} + \mu(\nabla \mathbf{u} + (\nabla \mathbf{u})^T)$ , where  $\mathbf{u}$  is the displacement, and  $\lambda$  and  $\mu$  are Lamé's parameters. We applied pure traction (aka Neumann) boundary conditions to (24), i.e.,

$$\sigma \cdot \mathbf{n} = \mathbf{t} \quad \text{on } \partial\Omega, \quad (25)$$

where  $\mathbf{n}$  and  $\mathbf{t}$  are unit outward surface normal and surface traction, respectively. Discretizing (24) and (25) using a Galerkin FEM leads to a singular system

$$\mathbf{K}\mathbf{u}_h = \mathbf{f}_h, \quad (26)$$

where the stiffness matrix  $\mathbf{K} \in \mathbb{R}^{n \times n}$  is symmetric positive semidefinite (SPSD), and  $\mathbf{u}_h$  and  $\mathbf{f}_h$  contain nodal values of  $\mathbf{u}$  and  $\mathbf{f}$ , respectively. The continuum equation is invariant to translation and rotation, so the null space of (26) is six dimensional. As in [52], we constructed the solid domain  $\Omega$  by first rotating a box  $[-1/4, 1/4] \times [-1/2, 1/2] \times [-1/8, 1/8]$  around  $x$ -,  $y$ -, and  $z$ -axes by  $\pi/2$ ,  $\pi/4$ ,  $\pi/5$  in that order and then by translating it by  $[0.1, 0.2, 0.3]^T$ . We discretized the domain using three linear tetrahedral meshes with 24,576, 196,608, and 2,058,000  $P_1$  elements, respectively. We computed the body force  $\mathbf{f}$  and surface traction  $\mathbf{h}$  using the manufactured solution  $\mathbf{u}(x, y, z) = \frac{1}{4}(\sin(\frac{\pi}{4}x), z^3, -y)$ . Due to discretization errors, the resulting linear system (26) may be inconsistent, which poses significant challenges for computing a stable solution for  $\mathbf{u}_h$ . Note that the nullspace of  $\mathbf{K}$  corresponds the rigid-body motion, of which an orthonormal basis may be computed analytically if the mesh and the finite-element basis functions are known; see e.g., [52]. However, an algebraic solver should be able to compute the nullspace from the matrix directly, for example, when the solver does not have access to the mesh or the basis functions.

To solve the inconsistent system, we use the solver *PIPIT* (or *PseudoInverse solver via Preconditioned Iterations*) [48], which is based on HIFIR and is composed of three steps:

- (1) Compute orthonormal basis  $\mathbf{V} \in \mathbb{R}^{n \times 6}$  of  $\mathcal{N}(\mathbf{K}^T) \equiv \mathcal{N}(\mathbf{K})$  for  $\mathbf{K}$  in (26) using HIFIR-preconditioned FGMRES.
- (2) Find a least-squares solution  $\mathbf{u}_{LS}$  of the consistent system  $\mathbf{K}\mathbf{u}_{LS} = (\mathbf{I} - \mathbf{V}\mathbf{V}^T)\mathbf{f}_h$  using HIF-preconditioned GMRES.
- (3) Obtain the pseudoinverse solution  $\mathbf{u}_{PI}$  via orthogonal projection, i.e.,  $\mathbf{u}_{PI} = (\mathbf{I} - \mathbf{V}\mathbf{V}^T)\mathbf{u}_{LS}$ .

All three steps reuse the same incomplete factorization. We refer readers to [48] for more detail. If the nullspace is known *a priori*, such as in [52], then Step 1 can be omitted. When computing the null-space vectors, we used FGMRES(30) with Householder QR for the Arnoldi process and terminated when the Hessenberg matrix became ill-conditioned. We used the default parameters (see Section 5.2) for HIFIR except that  $\text{rtol}$  was set to  $10^{-10}$  in step 2. For these meshes, HIF ended up having three, four, and five levels with nnz ratios 8.84, 10.4, and 10.7, respectively. Table 3 summarizes the timing results of PIPIT for these singular systems. As a point of reference, we used LSMR [30] preconditioned with RIF [12]. Since LSMR did not converge in our test without a preconditioner and a preconditioned LSMR can only compute a least-squares solution, we compare the computational cost of PIPIT for computing a least-squares solution (i.e., the factorization cost of HIF and step 2 of PIPIT) with RIF+LSMR. It can be seen that PIPIT was more than an order of magnitude more efficient than RIF+LSMR for the small and medium meshes. For the large mesh, RIF+LSMR failed to converge to the desired precision after 10,000 iterations. In addition, Table 3 also shows the runtimes for step 1 of PIPIT, which were comparable to solving for  $\mathbf{u}_{LS}$  since the same HIF preconditioner was reused. In addition, we report the accuracy of the first ( $\mathbf{v}_1$ ) and sixth ( $\mathbf{v}_6$ ) null-space vectors as examples, both of which converted to (near) machine precision. Note that for RIF+LSMR to compute  $\mathbf{u}_{PI}$  instead of  $\mathbf{u}_{LS}$ , it would also need to compute the null-space vectors, presumably using preconditioned LSMR [30], which could not converge at least for the largest system.



Table 3. Results for singular systems arising from linear elasticity with pure traction boundary conditions using  $P_1$  finite elements. We compare the costs of step 2 of PIPIT with RIF+LSMR, where leaders are in boldface and ‘–’ indicated non-convergence after 10,000 iterations. The last three columns show the cost and accuracy of null-space computations in step 1 of PIPIT. Times are in seconds.

mesh	$n$	nnz	PIPIT for $\mathbf{u}_{LS}$			RIF+LSMR for $\mathbf{u}_{LS}$			null-space computation		
			fac. time	tot. time	iter.	fac. time	tot. time	iter.	time	$\ \mathbf{K}\mathbf{v}_1\ /\ \mathbf{K}\ $	$\ \mathbf{K}\mathbf{v}_6\ /\ \mathbf{K}\ $
coarse	15,147	610,929	<b>3.5</b>	<b>3.82</b>	<b>15</b>	12.5	30.5	2,588	3.01	7e-16	3e-14
medium	109,395	4,652,505	<b>39.4</b>	<b>44</b>	<b>35</b>	308	741	8,673	126	3e-15	4e-16
fine	1,081,188	47,392,074	<b>511</b>	<b>700</b>	<b>152</b>	–	–	–	3.1e3	4e-15	6e-16

### 6.3 Stationary incompressible Navier–Stokes equations

As a third illustration, we solve the incompressible Navier–Stokes (INS) equations for modeling fluids. We consider the INS equations with normalized density on a domain  $\Omega \subset \mathbb{R}^3$ , which read

$$\mathbf{u}_t - \nu \Delta \mathbf{u} + \mathbf{u} \cdot \nabla \mathbf{u} + \nabla p = \mathbf{g}, \quad (27)$$

$$\nabla \cdot \mathbf{u} = 0, \quad (28)$$

where  $\mathbf{u}$  and  $p$  are velocities and pressure, respectively,  $\nu$  is the kinetic viscosity, and the subscript  $t$  denotes the temporal derivative. After dropping off the temporal-derivative term, we arrive at the stationary INS, for which the momentum equation (27) becomes

$$-\nu \Delta \mathbf{u} + \mathbf{u} \cdot \nabla \mathbf{u} + \nabla p = \mathbf{g}. \quad (29)$$

When integrating (27) in time, (29) is equivalent to having the time step equal to infinity. We discretize the INS in space using the  $P_2$ - $P_1$  Taylor–Hood (TH) elements [76], which leads to a system of nonlinear systems of equations. We then solve it using Newton–GMRES, an *inexact Newton method* [24] that uses the preconditioned GMRES in the inner iterations of Newton’s method. At iteration  $k$ , Newton’s method solves a linear problem

$$\mathbf{J}_k \begin{bmatrix} \delta \mathbf{u}_k \\ \delta p_k \end{bmatrix} \approx - \begin{bmatrix} \mathbf{f}_k \\ \mathbf{y}_k \end{bmatrix} \quad \text{with} \quad \mathbf{J}_k = \begin{bmatrix} \mathbf{K} + \mathbf{C}_k + \mathbf{W}_k & \mathbf{E}^T \\ \mathbf{E} & 0 \end{bmatrix}, \quad (30)$$

where  $\mathbf{K}$ ,  $\mathbf{E}$ ,  $\mathbf{C}_k$ , and  $\mathbf{W}_k$  correspond to  $\nu \Delta \delta \mathbf{u}$ ,  $\nabla \cdot \delta \mathbf{u}$ ,  $\mathbf{u}_k \cdot \nabla \delta \mathbf{u}$ , and  $\delta \mathbf{u} \cdot \nabla \mathbf{u}_k$ , respectively, and  $\delta \mathbf{u}_k$  and  $\delta p_k$  denote increments in velocity and pressure, respectively. Since  $\mathbf{J}_k$  is fairly dense in Newton’s method, we constructed a “sparsifier”  $\mathbf{B}_k$  by omitting  $\mathbf{W}_k$  when building the preconditioner. For robustness, we start with Picard iterations, which uses  $\mathbf{B}_k$  in place of  $\mathbf{J}_k$  at each Newton’s step, and then switch to Newton’s iterations once the solution is sufficiently accurate. For the initial guess  $[\mathbf{u}_0, p_0]^T$ , we obtained it by solving the corresponding Stokes equation, i.e.,  $-\nu \Delta \mathbf{u} + \nabla p = \mathbf{g}$ . For more details, see [21].

As a demonstration, we solved the 3D flow-over-cylinder benchmark problem [73], where a cylinder of diameter  $D = 0.1$  is placed in a channel of length 2.5 with square cross-sections of height  $H = 0.41$ . The inflow boundary condition is imposed on the left side of a box, which reads  $\mathbf{u}_{\text{in}} = (U(y, z), 0, 0)$ , where  $U(y, z) = 16 \times 0.45 yz(H - y)(H - z)/H^4$ . A “do-nothing” velocity is imposed for the outflow (right face) along with a zero pressure. The rest boundaries are no-slip walls. The kinetic viscosity was  $\nu = 1 \times 10^{-3}$ , so the Reynolds number is  $\text{Re} = 4 \times 0.45 D / (9 \nu) = 20$ . We generated three sets of unstructured tetrahedral meshes using Gmsh [32], with 71,031, 268,814, and 930,248 elements, respectively. Figure 5 shows a coarse sample mesh along with the computed speed. We assembled the matrices  $\mathbf{J}_k$  and  $\mathbf{B}_k$  using our in-house FEM code. Table 4 shows the performance of HIF+GMRES(30) for a representative Newton step, with  $\text{rtol} = 10^{-6}$  in GMRES and  $\tau = 10^{-2}$ ,  $\kappa = 5$ , and  $\alpha = 3$  for HIF. As a point of reference, we solved the same systems

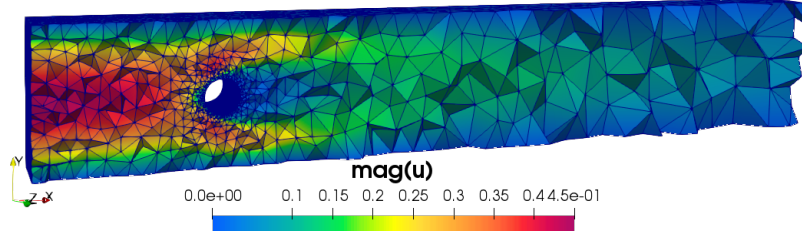


Fig. 5. Cut-off view of the speed for the 3D flow-over-cylinder problem with a coarse sample mesh.

Table 4. Results for stationary INS with TH elements in one representative Newton's step solved by GMRES(3) preconditioned by HIF on the sparsifier  $B_k$  in comparison with ILUPACK. 'x' indicates out of memory. Times are in seconds. Leaders are in boldface.

mesh	$n$	$\text{nnz}(J_k)$	$\text{nnz}(B_k)$	HIF+GMRES(30)				ILUPACK+GMRES(30)			
				nnz rat.	fac. time	tot. time	iter.	nnz rat.	fac. time	tot. time	iter.
coarse	262,912	21,870,739	9,902,533	3.47	<b>20.3</b>	<b>22.6</b>	17	8.34	130	133	<b>11</b>
medium	1,086,263	98,205,997	43,686,979	3.4	<b>106</b>	<b>124</b>	33	13.4	1.92e3	1.94e3	<b>14</b>
fine	3,738,327	343,357,455	152,438,721	3.47	<b>442</b>	<b>586</b>	<b>68</b>	x	x	x	x

using ILUPACK [15] with  $\text{droptol} = 10^{-2}$  and other default parameters. As we can see, HIF-preconditioned GMRES performed consistently well, even for the finest mesh. Its overall performance was faster than ILUPACK by a factor about six and 16 for the coarse and intermediate-level meshes, although ILUPACK used fewer GMRES iterations. More importantly, ILUPACK ran out of the 64 GB main memory for the largest problem. In [21], we also compared HIF with the direct solve MUMPS [3], which also ran out of memory for the largest case as ILUPACK, and with ILU(1) and ILU(2), for which GMRES failed to converge.

#### 6.4 Advection-diffusion equation with fully implicit Runge-Kutta schemes

As our final illustration, we consider the time-dependent advection-diffusion (AD) equation for  $u: \Omega \times [0, T] \rightarrow \mathbb{R}$ ,

$$u_t - \mu \Delta u + \mathbf{v} \cdot \nabla u = f, \quad (31)$$

where  $\mu \geq 0$  is the diffusion coefficient,  $\mathbf{v}$  is a divergence-free velocity field, and  $f$  is some source term. As a demonstration, we chose  $\Omega = [0, 1]^3$  and computed  $f$  and the Dirichlet boundary conditions from the manufactured solution  $u(x, y, z, t) = \sin(1.5\pi t) \sin(\pi x) \sin(\pi y) \sin(\pi z)$ . We used the fourth and sixth-order finite difference method (FDM) to discretize (31), leading to the semi-discretization form

$$\mathbf{u}_t(t) = \mathbf{J}\mathbf{u}(t) + \mathbf{f}(t), \quad (32)$$

where  $\mathbf{J} \in \mathbb{R}^{n \times n}$  denotes the Jacobian matrix corresponding to the operator  $(\mu \Delta - \mathbf{v} \cdot \nabla)$ . Eq. (32) is a system of stiff ordinary differential equations (ODEs) and can be integrated using high-order fully implicit Runge-Kutta (FIRK) schemes, such as  $s$ -stage Gauss-Legendre schemes, which are  $2s$ -order accurate and are unconditionally stable. A

Runge-Kutta scheme can be expressed by the Butcher tableau  $\begin{array}{c|c} \mathbf{c} & \mathbf{A} \\ \hline & \mathbf{b}^T \end{array}$ , where  $\mathbf{A} \in \mathbb{R}^{s \times s}$ ,  $\mathbf{c} \in \mathbb{R}^s$ , and  $\mathbf{b} \in \mathbb{R}^s$  [17].

Given a time step  $\delta t$ , Eq. (32) leads to an  $sn \times sn$  linear system

$$\mathcal{A}\mathcal{K} = \mathcal{B} \quad \text{with} \quad \mathcal{A} = \mathbf{I}_{sn} - \delta t \mathbf{A} \otimes \mathbf{J}, \quad (33)$$

Table 5. Results for solving the advection-diffusion equation with fourth- and sixth-order FDM and two- and four-stage Gauss–Legendre schemes correspondingly, using GMRES(30) right-preconditioned by HIF-based and ILU(0)-based BCSD. Times are in seconds. ‘–’ indicates that GMRES failed to converge after 500 iterations. Leaders are in boldface.

$h$	$n$	nnz	BCSD with HIF				BCSD with ILU(0)+pre			
			nnz ratio	fac. time	tot. time	iter.	nnz ratio	fac. time	tot. time	iter.
Two-stage Gauss–Legendre scheme with fourth-order finite differences										
1/32	29,791	381,517	5.47	1.08	1.52	<b>17</b>	1.0	<b>0.1</b>	<b>1.31</b>	66
1/64	250,047	3,226,797	5.27	11.0	<b>19.5</b>	<b>34</b>	1.0	<b>0.89</b>	23.8	161
1/128	2,048,383	26,532,205	5.27	104	<b>262</b>	<b>77</b>	1.0	<b>8.05</b>	566	398
Four-stage Gauss–Legendre scheme with sixth-order finite differences										
1/32	29,791	560,263	5.64	3.56	<b>4.77</b>	<b>16</b>	1.0	<b>0.59</b>	6.57	144
1/64	250,047	4,727,079	5.38	35.7	<b>57.0</b>	<b>31</b>	1.0	<b>2.77</b>	95.4	257
1/128	2,048,383	38,822,503	5.37	343	<b>805</b>	<b>75</b>	1.0	–	–	–

where  $I_m$  denotes the  $m$ -dimension identity matrix,  $\otimes$  denotes the Kronecker-product operator,  $\mathcal{A} \in \mathbb{R}^{sn \times sn}$ ,  $\mathcal{B} \in \mathbb{R}^{sn}$ , and  $\mathcal{K} \in \mathbb{R}^{sn}$ . We refer readers to [49] for more details.

To assess HIF for complex-valued matrices, we use an optimal preconditioner, called *block CSD* or *BCSD*, developed in [49]. BCSD is based on the complex Schur decomposition (CSD) of the Butcher matrix  $A$  (i.e.,  $A = QUQ^H$ , where  $Q \in \mathbb{C}^{s \times s}$  is unitary and  $U \in \mathbb{C}^{s \times s}$  is upper triangular), and it reads

$$\mathcal{M} = (Q \otimes I_n) \mathcal{U} (Q^H \otimes I_n) \quad \text{with} \quad \mathcal{U} = I_{sn} - \delta t U \otimes J. \quad (34)$$

$\mathcal{M}$  is optimal in that  $\mathcal{A}\mathcal{M}^{-1} = I_{sn}$ , where  $\mathcal{M}^{-1} = (Q \otimes I_n) \mathcal{U}^{-1} (Q^H \otimes I_n)$ ; see [49] for more details. Note that  $\mathcal{U}$  in (34) is block upper triangular, so computing  $\mathcal{U}^{-1}\mathcal{X}$  for a vector  $\mathcal{X}$  only requires (approximately) factorizing the diagonal blocks of  $\mathcal{U}$ , i.e.,  $\mathcal{M}_i = I_n - \delta t \lambda_i J \in \mathbb{C}^{n \times n}$  for  $i = 1, 2, \dots, s$ , where  $\lambda_i \in \mathbb{C}$  are the diagonal entries of  $U$ , which are the eigenvalues of  $A$ . For Gauss–Legendre schemes, there are  $\lfloor s/2 \rfloor$  distinct conjugate pairs of complex eigenvalues of  $A$ , and given  $\mathcal{M}_i \in \mathbb{C}^{n \times n}$ ,  $\mathbf{y} = \mathcal{M}_i^{-1} \mathbf{x} \implies \bar{\mathbf{y}} = \overline{\mathcal{M}_i^{-1} \mathbf{x}}$ . Hence, we only need to factorize  $\lfloor s/2 \rfloor$  distinct complex-valued diagonal blocks for BCSD. We constructed the blocks in the Jacobian matrices  $J$  in (32) using our in-house high-order FDM code on equidistant structured grids with grid sizes  $h = 1/32, 1/64, 1/128$  and a velocity field  $\mathbf{v} = [1, 1, 1]^T$ . We factorized  $\mathcal{M}_i$  using double-precision complex HIF with parameters  $\tau = 10^{-3}$ ,  $\kappa = 5$ , and  $\alpha = 5$ . With these parameters, HIF ended up producing three to four levels. Table 5 shows the performance of HIF-based BCSD preconditioner for the two- and four-stage Gauss–Legendre schemes for the first time step with  $\delta t = 1/8$ . As a point of reference, Table 5 also reports the results using MATLAB’s built-in (precompiled) `ilu` function without fills (aka ILU(0)) with preprocessing steps (including equilibration [26] and fill-reduction reordering [19]). We chose ILU(0) as a baseline since it is commonly used in the literature for the diagonal blocks [50, 65]. It can be seen HIF was significantly faster than ILU(0) overall, although ILU(0) was more efficient in terms of factorization cost. In addition, BCSD with ILU(0) failed to converge for the largest case. In [49], we also compared HIF with BoomerAMG in hypre v2.21.0 [45] for some real-valued block preconditioners, and HIF was about a factor of eight faster than BoomerAMG for larger problems. We do not compare BoomerAMG for BCSD, since hypre does not yet support complex arithmetic.

## 7 CONCLUSION AND FUTURE WORK

In this work, we introduced a software package, *HIFIR*, for preconditioning GMRES and FGMRES for solving unsymmetric sparse linear systems. Unlike previous software packages, HIFIR is designed to solve singular and near-singular (aka

ill-conditioned) systems, including finding least-squares solutions for consistent singular systems, null-space vectors of singular matrices, and pseudoinverse solutions for inconsistent systems. This unique feature is backed by a new theory of  $\epsilon$ -accurate AGI, and a new algorithm that combines multilevel incomplete LU factorization with an RRQR on the final Schur complement. Compared to its predecessor HILUCSI, *HIFIR* also introduces an algorithmic innovation, namely IBRR, which improves the robustness and significantly reduces the size of the final Schur complement for some systems. *HIFIR* was implemented in C++, with user-friendly high-level interfaces for MATLAB and Python in *hifir4m* and *hifir4py*, respectively. We have released them as open-source software. We described the software design of *HIFIR* in terms of its efficient data structures and its template-based generic programming interfaces for mixed-precision real and complex values. We also demonstrated the effectiveness of *HIFIR* for ill-conditioned or singular systems arising from several applications, including the Helmholtz equation, linear elasticity, incompressible Navier–Stokes equations, and advection-diffusion equation. As presented in this work, *HIFIR* was serial. However, it can be used as the computational kernel in a domain-decomposition preconditioner [75] by factorizing the diagonal blocks within each processor. In addition, we are presently developing a multi-threaded implementation with the option of applying the multilevel solver and multilevel matrix-vector multiplication on GPUs, which we plan to release in the future.

## ACKNOWLEDGMENTS

Computational results were obtained using the Seawulf cluster at the Institute for Advanced Computational Science of Stony Brook University, which was partially funded by the Empire State Development grant NYS #28451.

## REFERENCES

- [1] Martin Alnæs, Jan Blechta, Johan Hake, August Johansson, Benjamin Kehlet, Anders Logg, Chris Richardson, Johannes Ring, Marie E Rognes, and Garth N Wells. 2015. The FEniCS project version 1.5. *Arch. Numer. Softw.* 3, 100 (2015).
- [2] Patrick R Amestoy, Timothy A Davis, and Iain S Duff. 2004. Algorithm 837: AMD, an approximate minimum degree ordering algorithm. *ACM Trans. Math. Software* 30, 3 (2004), 381–388.
- [3] Patrick R Amestoy, Iain S Duff, Jean-Yves L'Excellent, and Jacko Koster. 2000. MUMPS: A general purpose distributed memory sparse solver. In *International Workshop on Applied Parallel Computing*. Springer, 121–130.
- [4] James Baglama and Lothar Reichel. 2005. Augmented implicitly restarted Lanczos bidiagonalization methods. *SIAM J. Sci. Comput.* 27, 1 (2005), 19–42.
- [5] Satish Balay, Shrirang Abhyankar, Mark F. Adams, Jed Brown, Peter Brune, Kris Buschelman, Lisandro Dalcin, Alp Dener, Victor Eijkhout, William D. Gropp, Dmitry Karpeyev, Dinesh Kaushik, Matthew G. Knepley, Dave A. May, Lois Curfman McInnes, Richard Tran Mills, Todd Munson, Karl Rupp, Patrick Sanan, Barry F. Smith, Stefano Zampini, Hong Zhang, and Hong Zhang. 2020. *PETSc Users Manual*. Technical Report ANL-95/11 - Revision 3.14. Argonne National Laboratory. <https://www.mcs.anl.gov/petsc>
- [6] Randolph E Bank and Craig C Douglas. 1993. Sparse matrix multiplication package (SMMP). *Adv. Comput. Math.* 1, 1 (1993), 127–137.
- [7] Stefan Behnel, Robert Bradshaw, Craig Citro, Lisandro Dalcin, Dag Sverre Seljebotn, and Kurt Smith. 2010. Cython: The best of both worlds. *Comput. Sci. Eng.* 13, 2 (2010), 31–39.
- [8] Michele Benzi. 2002. Preconditioning techniques for large linear systems: a survey. *J. Comput. Phys.* 182, 2 (2002), 418–477.
- [9] Michele Benzi and Maxim A Olshanskii. 2006. An augmented Lagrangian-based approach to the Oseen problem. *SIAM J. Sci. Comput.* 28, 6 (2006), 2095–2113.
- [10] Michele Benzi, Daniel B Szyld, and Arno Van Duin. 1999. Orderings for incomplete factorization preconditioning of nonsymmetric problems. *SIAM J. Sci. Comput.* 20, 5 (1999), 1652–1670.
- [11] Michele Benzi and Miroslav Tuma. 2003. A robust incomplete factorization preconditioner for positive definite matrices. *Numer. Linear Algebra Appl.* 10, 5-6 (2003), 385–400.
- [12] Michele Benzi and Miroslav Tuma. 2003. A robust preconditioner with low memory requirements for large sparse least squares problems. *SIAM J. Sci. Comput.* 25, 2 (2003), 499–512.
- [13] Christian H. Bischof. 1990. Incremental Condition Estimation. *SIAM J. Matrix Anal. Appl.* 11, 2 (1990), 312–322.
- [14] Åke Björck. 1996. *Numerical Methods for Least Squares Problems*. SIAM.
- [15] Matthias Bollhöfer, José I Aliaga, Alberto F Martín, and Enrique S Quintana-Orti. 2011. ILUPACK. In *Encyclopedia of Parallel Computing*. Springer, 917–926.

- [16] Matthias Bollhöfer and Yousef Saad. 2006. Multilevel preconditioners constructed from inverse-based ILUs. *SIAM J. Sci. Comput.* 27, 5 (2006), 1627–1650.
- [17] John Charles Butcher and Nicolette Goodwin. 2008. *Numerical Methods for Ordinary Differential Equations*. Vol. 2. Wiley Online Library.
- [18] Tony F Chan. 1987. Rank revealing QR factorizations. *Linear Algebra Appl.* 88 (1987), 67–82.
- [19] Wing-Man Chan and Alan George. 1980. A linear time implementation of the reverse Cuthill-McKee algorithm. *BIT Numer. Math.* 20, 1 (1980), 8–14.
- [20] Qiao Chen, Aditi Ghai, and Xiangmin Jiao. 2021. HILUCSI: Simple, robust, and fast multilevel ILU for large-scale saddle-point problems from PDEs. *Numer. Linear Algebra Appl.* 28, 6 (2021), e2400. <https://doi.org/10.1002/nla.2400>
- [21] Qiao Chen, Xiangmin Jiao, and Oliver Yang. 2021. Robust and efficient multilevel-ILU preconditioning of hybrid Newton–GMRES for incompressible Navier–Stokes equations. *Int. J. Numer. Methods Fluids* 93, 12 (2021), 3405–3423. <https://doi.org/10.1002/fld.5039>
- [22] Edmond Chow and Yousef Saad. 1997. Experimental study of ILU preconditioners for indefinite matrices. *J. Comput. Appl. Math.* 86, 2 (1997), 387–414.
- [23] Timothy A Davis and Yifan Hu. 2011. The University of Florida sparse matrix collection. *ACM Trans. Math. Softw.* 38, 1 (2011), 1–25.
- [24] Ron S Dembo, Stanley C Eisenstat, and Trond Steihaug. 1982. Inexact Newton methods. *SIAM J. Numer. Anal.* 19, 2 (1982), 400–408.
- [25] James W. Demmel, Michael T. Heath, and Henk A. van der Vorst. 1993. Parallel numerical linear algebra. *Acta Numer.* 2 (1993), 111–197. <https://doi.org/10.1017/S096249290000235X>
- [26] Iain S Duff and Jacko Koster. 2001. On algorithms for permuting large entries to the diagonal of a sparse matrix. *SIAM J. Matrix Anal. Appl.* 22, 4 (2001), 973–996.
- [27] Stanley C Eisenstat, Martin H Schultz, and Andrew H Sherman. 1981. Algorithms and data structures for sparse symmetric Gaussian elimination. *SIAM J. Sci. Stat. Comp.* 2, 2 (1981), 225–237.
- [28] Howard Elman, Victoria E Howle, John Shadid, Robert Shuttleworth, and Ray Tuminaro. 2006. Block preconditioners based on approximate commutators. *SIAM J. Sci. Comput.* 27, 5 (2006), 1651–1668.
- [29] Oliver G Ernst and Martin J Gander. 2012. Why it is difficult to solve Helmholtz problems with classical iterative methods. In *Numerical Analysis of Multiscale Problems*. Springer, 325–363.
- [30] David Chin-Lung Fong and Michael Saunders. 2011. LSMR: An iterative algorithm for sparse least-squares problems. *SIAM J. Sci. Comput.* 33, 5 (2011), 2950–2971.
- [31] John Alan George. 1971. *Computer implementation of the finite element method*. Ph.D. Dissertation. Stanford University, Stanford, CA, USA. AAI7205916.
- [32] Christophe Geuzaine and Jean-François Remacle. 2009. Gmsh: A 3-D finite element mesh generator with built-in pre-and post-processing facilities. *Int. J. Numer. Meth. Eng.* 79, 11 (2009), 1309–1331.
- [33] Aditi Ghai, Cao Lu, and Xiangmin Jiao. 2019. A comparison of preconditioned Krylov subspace methods for large-scale nonsymmetric linear systems. *Numer. Linear Algebra Appl.* 26, 1 (2019), e2215.
- [34] Gene H. Golub and Charles F. Van Loan. 2013. *Matrix Computations* (4th ed.). Johns Hopkins.
- [35] Nicholas Gould and Jennifer Scott. 2017. The state-of-the-art of preconditioners for sparse linear least-squares problems. *ACM Trans. Math. Softw.* 43, 4 (2017), 1–35.
- [36] Gaël Guennebaud, Benoît Jacob, et al. 2010. Eigen v3. <http://eigen.tuxfamily.org>
- [37] Anshul Gupta. 2021. *WSMP: Watson Sparse Matrix Package (Part-III: iterative solution of sparse systems) Version 20.12*. Technical Report. IBM T. J. Watson Research Center. <http://www.research.ibm.com/projects/wsmpp>.
- [38] Anshul Gupta and Thomas George. 2010. Adaptive techniques for improving the performance of incomplete factorization preconditioning. *SIAM J. Sci. Comput.* 32, 1 (2010), 84–110.
- [39] Anshul Gupta, Mahesh Joshi, and Vipin Kumar. 2001. *WSMP: a high-performance shared- and distributed-memory parallel sparse linear equation solver*. Technical Report. IBM T. J. Watson Research Center.
- [40] Ken Hayami, Jun-Feng Yin, and Tokushi Ito. 2010. GMRES methods for least squares problems. *SIAM J. Matrix Anal. Appl.* 31, 5 (2010), 2400–2430.
- [41] P. Heggernes, S. Eisenstat, G. Kumfert, and A. Pothén. 2001. The computational complexity of the minimum degree algorithm. In *Proceedings of 14th Norwegian Computer Science Conference*. 98–109.
- [42] Michael A Heroux, Roscoe A Bartlett, Vicki E Howle, Robert J Hoekstra, Jonathan J Hu, Tamara G Kolda, Richard B Lehoucq, Kevin R Long, Roger P Pawlowski, Eric T Phipps, et al. 2005. An overview of the Trilinos project. *ACM Trans. Math. Softw.* 31, 3 (2005), 397–423.
- [43] Magnus Rudolph Hestenes, Eduard Stiefel, et al. 1952. Methods of conjugate gradients for solving linear systems. *J. Res. Natl. Bur. Stand.* 49, 1 (1952), 409–436.
- [44] Charles AR Hoare. 1961. Algorithm 65: find. *Commun. ACM* 4, 7 (1961), 321–322.
- [45] hypre Developers. 2021. *hypre Documentation Release 2.21.0*. Lawrence Livermore National Laboratory.
- [46] Klaus Iglberger, Georg Hager, Jan Treibig, and Ulrich Rüde. 2012. Expression Templates Revisited: A Performance Analysis of Current Methodologies. *SIAM J. Sci. Comput.* 34, 2 (2012), C42–C69.
- [47] A. Jennings and M. A. Ajiz. 1984. Incomplete methods for solving  $A^T Ax = b$ . *SIAM J. Sci. Comput.* 5, 4 (1984), 978–987.
- [48] Xiangmin Jiao and Qiao Chen. 2021. Approximate generalized inverses with iterative refinement for  $\epsilon$ -accurate preconditioning of singular systems. *SIAM J. Matrix Anal. Appl.* (2021). To appear.

- [49] Xiangmin Jiao, Xuebin Wang, and Qiao Chen. 2021. Optimal and low-memory near-optimal preconditioning of fully implicit Runge-Kutta schemes for parabolic PDEs. *SIAM J. Sci. Comput.* 43, 5 (2021), A3527–A3551. <https://doi.org/10.1137/20M1387985>
- [50] Alex Kanevsky, Mark H. Carpenter, David Gottlieb, and Jan S. Hesthaven. 2007. Application of implicit-explicit high order Runge–Kutta methods to discontinuous-Galerkin schemes. *J. Comput. Phys.* 225, 2 (2007), 1753–1781. <https://doi.org/10.1016/j.jcp.2007.02.021>
- [51] David Kay, Daniel Loghin, and Andrew Wathen. 2002. A preconditioner for the steady-state Navier–Stokes equations. *SIAM J. Sci. Comput.* 24, 1 (2002), 237–256.
- [52] Miroslav Kuchta, Kent-Andre Mardal, and Mikael Mortensen. 2019. On the singular Neumann problem in linear elasticity. *Numer. Linear Algebra Appl.* 26, 1 (2019), e2212.
- [53] STFC Rutherford Appleton Laboratory. 2021. HSL\_MC64. Permute and scale a sparse unsymmetric or rectangular matrix to put large entries on the diagonal. [https://www.hsl.rl.ac.uk/catalogue/hsl\\_mc64.html](https://www.hsl.rl.ac.uk/catalogue/hsl_mc64.html) Accessed: 2021-3-16.
- [54] Na Li and Yousef Saad. 2005. Crout versions of ILU factorization with pivoting for sparse symmetric matrices. *Electron. Trans. Numer. Anal.* 20 (2005), 75–85.
- [55] Na Li, Yousef Saad, and Edmond Chow. 2003. Crout versions of ILU for general sparse matrices. *SIAM J. Sci. Comput.* 25, 2 (2003), 716–728.
- [56] Xiaoye S Li. 2005. An overview of SuperLU: Algorithms, implementation, and user interface. *ACM Trans. Math. Softw.* 31, 3 (2005), 302–325.
- [57] Xiaoye S Li and Meiyue Shao. 2011. A supernodal approach to incomplete LU factorization with partial pivoting. *ACM Trans. Math. Softw.* 37, 4 (2011), 1–20.
- [58] Anders Logg and Garth N Wells. 2010. DOLFIN: Automated finite element computing. *ACM Trans. Math. Softw.* 37, 2 (2010), 1–28.
- [59] Jan Mayer. 2006. Alternative weighted dropping strategies for ILUTP. *SIAM J. Sci. Comput.* 27, 4 (2006), 1424–1437.
- [60] Jan Mayer. 2007. ILU++: A new software package for solving sparse linear systems with iterative methods. In *PAMM: Proceedings in Applied Mathematics and Mechanics*, Vol. 7. Wiley Online Library, 2020123–2020124.
- [61] Keiichi Morikuni and Ken Hayami. 2015. Convergence of inner-iteration GMRES methods for rank-deficient least squares problems. *SIAM J. Matrix Anal. Appl.* 36, 1 (2015), 225–250.
- [62] Johann Moulin, Pierre Jolivet, and Olivier Marquet. 2019. Augmented Lagrangian preconditioner for large-scale hydrodynamic stability analysis. *Comput. Methods Appl. Mech. Eng.* 351 (2019), 718–743.
- [63] Christopher C Paige and Michael A Saunders. 1975. Solution of sparse indefinite systems of linear equations. *SIAM J. Numer. Anal.* 12, 4 (1975), 617–629.
- [64] Christopher C Paige and Michael A Saunders. 1982. LSQR: An algorithm for sparse linear equations and sparse least squares. *ACM Trans. Math. Softw.* 8, 1 (1982), 43–71.
- [65] Will Pazner and Per-Olof Persson. 2017. Stage-parallel fully implicit Runge–Kutta solvers for discontinuous Galerkin fluid simulations. *J. Comput. Phys.* 335 (2017), 700–717. <https://doi.org/10.1016/j.jcp.2017.01.050>
- [66] George Poole and Larry Neal. 2000. The rook’s pivoting strategy. *J. Comput. Appl. Math.* 123, 1-2 (2000), 353–369.
- [67] C Radhakrishna Rao, Sujit Kumar Mitra, et al. 1972. Generalized inverse of a matrix and its applications. In *Proceedings of the Sixth Berkeley Symposium on Mathematical Statistics and Probability, Volume 1: Theory of Statistics*. The Regents of the University of California, 601–620.
- [68] Youcef Saad. 1988. Preconditioning techniques for nonsymmetric and indefinite linear systems. *J. Comp. Appl. Math.* 24, 1-2 (1988), 89–105.
- [69] Youcef Saad. 1993. A flexible inner-outer preconditioned GMRES algorithm. *SIAM J. Sci. Comput.* 14, 2 (1993), 461–469.
- [70] Yousef Saad. 2003. *Iterative Methods for Sparse Linear Systems*. SIAM.
- [71] Youcef Saad and Martin H Schultz. 1986. GMRES: A generalized minimal residual algorithm for solving nonsymmetric linear systems. *SIAM J. Sci. Comput.* 7, 3 (1986), 856–869.
- [72] Yousef Saad and Brian Suchoamel. 2002. ARMS: An algebraic recursive multilevel solver for general sparse linear systems. *Numer. Linear Algebra Appl.* 9, 5 (2002), 359–378.
- [73] Michael Schäfer, Stefan Turek, Franz Durst, Egon Krause, and Rolf Rannacher. 1996. Benchmark computations of laminar flow around a cylinder. In *Flow Simulation with High-Performance Computers II*. Springer, 547–566.
- [74] David Silvester, Howard Elman, David Kay, and Andrew Wathen. 2001. Efficient preconditioning of the linearized Navier–Stokes equations for incompressible flow. *J. Comput. Appl. Math.* 128, 1-2 (2001), 261–279.
- [75] Barry F. Smith, Petter E. Bjørstad, and William D. Gropp. 1996. *Domain Decomposition: Parallel Multilevel Methods for Elliptic Partial Differential Equations*. Cambridge University Press.
- [76] Cedric Taylor and Paul Hood. 1973. A numerical solution of the Navier–Stokes equations using the finite element technique. *Comput. Fluids* 1, 1 (1973), 73–100.
- [77] Pauli Virtanen, Ralf Gommers, Travis E. Oliphant, Matt Haberland, Tyler Reddy, David Cournapeau, Evgeni Burovski, Pearu Peterson, Warren Weckesser, Jonathan Bright, Stéfan J. van der Walt, Matthew Brett, Joshua Wilson, K. Jarrod Millman, Nikolay Mayorov, Andrew R. J. Nelson, Eric Jones, Robert Kern, Eric Larson, C J Carey, İlhan Polat, Yu Feng, Eric W. Moore, Jake VanderPlas, Denis Laxalde, Josef Perktold, Robert Cimrman, Ian Henriksen, E. A. Quintero, Charles R. Harris, Anne M. Archibald, Antônio H. Ribeiro, Fabian Pedregosa, Paul van Mulbregt, and SciPy 1.0 Contributors. 2020. SciPy 1.0: Fundamental Algorithms for Scientific Computing in Python. *Nature Methods* 17 (2020), 261–272. <https://doi.org/10.1038/s41592-019-0686-2>

## A FLEXIBLE ARRAY-BASED SPARSE MATRIX DATA STRUCTURE

We describe a flexible, three-tiered, array-based (instead of pointer-based) sparse matrix data structure to support fan-in updates, deferring, and rook pivoting, respectively. We focus on the column-oriented version for  $L$ ; the data structure for  $U$  uses a corresponding row-oriented version.

### A.1 Partially augmented CSC for fan-in updates

We first briefly describe the baseline data structure as in [55], which extends the standard CSC format. Recall that the CSC format has the following three arrays:

- `val`: a floating-point array of size equal to the total number of nonzeros, with nonzeros stored column by column;
- `row_ind`: an integer array of size equal to that of `row_ind`, storing the row indices in each column;
- `col_start`: an integer array of size  $n+1$ , storing the starting index of each column in `row_ind`, where `col_start` ( $k$ ) stores the starting position for the  $k$ th column in `row_ind`.

To support fan-in update in Algorithm 1, we maintain two additional arrays `Lstart` and `Llist` as in [55], where `Lstart` is a size- $n$  integer array storing the first entry in each column of  $L$  whose row index is no smaller than  $k$  at the  $k$ th step, and `Llist` is a size- $n$  array-based linked list storing the index of each column that has a nonzero entry in  $\ell_k^T$ . The combination of `Lstart` and `Llist` allows efficient access of the  $k$ th row in  $L$ . We refer to this baseline data structure as *partially augmented CSC (PACSC)*. The data structure for  $U$  uses the counterpart *PACSR*, which partially augments CSR.

### A.2 Partially augmented CSC with gaps

PACSC is memory efficient, but it does not support permutations, such as static or dynamic deferring. To support static and dynamic deferring, we extend the data structure to allow a “gap” of size  $d$  between  $L_B$  and  $L_E$  if there have been  $d$  deferrals. We maintain the gap as follows. At the  $k$ th step, suppose there have been  $d-1$  deferrals in the preceding steps. Before performing computation on the  $k$ th row, we first move  $\ell_{k+d-1}^T$  to  $\ell_k^T$  in  $L$  to eliminate the gap. If row  $k$  needs to be deferred, we directly move the row from  $\ell_{k+d-1}^T$  to row  $\ell_{n+d}^T$  in  $L$ , which increases the gap to  $d$ . Figure 6 illustrates these operations. To avoid dynamic expansion of the arrays, we pre-allocate the CSC storage to allow up to  $2n$  rows, and also enlarge `Llist` and `Ulist` to size  $2n$ . At the end of `ilu_factorize`, we eliminate the gap by moving  $L_{n_1+d:n+d}$  to  $L_{n_1:n}$ . We refer to the above data structure as *PACSC-G*; the data structure for  $U$  uses the corresponding *PACSR-G*. It is worth noting that in Algorithm 1, row  $i$  in  $L$  for  $i > k$  refers to row  $i+d$  in PACSC-G, and similarly, column  $j$  in  $U$  for  $j > k$  refers to column  $j+d$  in PACSR-G. Note that ILUPACK [15] also extended CSC to support deferring, but we could not find its implementation details in its documentation for comparison.

### A.3 Fully augmented CSC for rook pivoting

To support row interchanges of  $L$  in rook pivoting, we need to access its  $i$ th row for  $k \leq i \leq n_1$ . The PACSC (with or without gap) is insufficient for this purpose. To support rook pivoting, we need to access any row in  $L_{k:n_1:k}$  and any column in  $U_{1:k,k:n}$ . To support this, we replace the `Lstart` and `Llist` arrays in PACSC with the following additional arrays, analogous to those in the CSR (Compressed Sparse Row) format:

- `val_pos`: an integer array of size equal to the total number of nonzeros, storing the indices of the nonzeros in the `val` array in the underlying CSC format;
- `inv_val_pos`: an integer array storing the inverse mapping of `val_pos`.
- `col_ind`: an integer array of size equal to that of `val_pos`, storing the column indices within `val_pos` in each row;

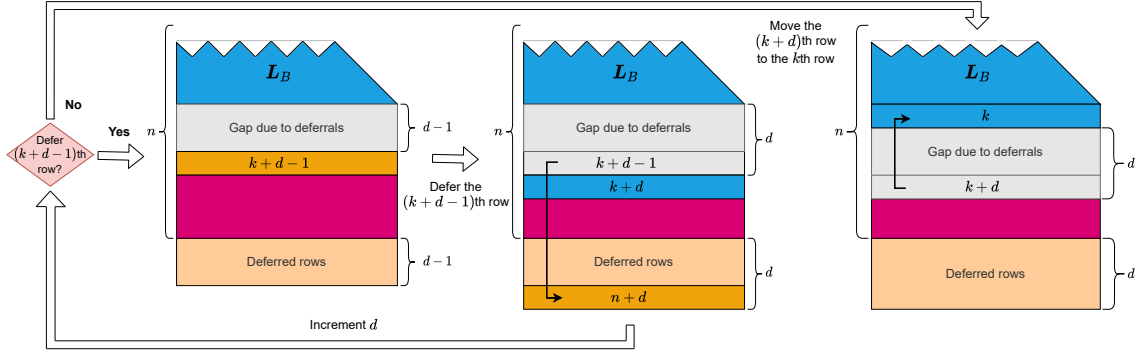


Fig. 6. Illustration of PACSC-G (partially augmented CSC with gap). The left panel shows a gap of  $d - 1$  before step  $k$  of fan-in ILU; the middle panel defers the  $k$ th row stored in the  $(k + d - 1)$ th position to the end of  $L_B$ ; the right panel moves the  $k$ th row from the  $(k + d)$ th position to the end of  $L_B$  for computation.

- `row_start`: an integer array of size  $n$ , storing the starting index of each row in `col_ind`;
- `row_next`: an integer array of the same size as `col_ind`, storing the index in `col_ind` for the next nonzero in the same row;
- `row_end`: an integer array of size  $n$ , storing the last index of each row in `col_ind`.

We refer to this data structure as the *fully augmented CSC* (or *FACSC*). Here, `val_pos` and `inv_val_pos` play the same role as `val` in CSR; we introduced them to avoid duplicating the numerical values. `col_ind` and `row_start` play the same roles as their respective counterparts in CSR. The arrays `row_next` and `row_end` essentially maintain Llist for all rows in  $L_{k:n,1:k}$  instead of for just the  $k$ th row. When interchanging rows  $i$  and  $r$  in  $L$  during pivoting, besides updating `val` and `row_ind` in CSC, we need to swap `row_start(i)` and `row_end(i)` with `row_start(r)` and `row_end(r)`, respectively, while keeping the other arrays intact. The data structure for  $U$  uses *FACSR*, which fully augments CSR.

## B TIME COMPLEXITY OF INVERSE-BASED ROK PIVOTING

We analyze the time complexity for partial row interchanges in  $L$ ; the analysis for column interchanges in  $U$  is similar. In Algorithm 2, there are three key steps: 1) computing the  $k$ th column vector  $\hat{\ell}$  (line 2), 2) finding a potential pivot  $r$  (line 3), and 3) interchanging the  $k$ th and  $r$ th rows in  $L$  (line 5). The total number of floating-point operations in computing  $\hat{\ell}$  is bounded by  $O\left(\text{nnz}(\hat{a}_{p_k}) + \sum_{i \in \text{nnz}(u_k)} \text{nnz}(L_{k+1:n,i})\right)$ . Under the assumption that the averaged number of nonzeros per row and column in the input is a constant (say, bounded by  $C$ ), the scalability-oriented dropping ensures that this cost is also bounded by a constant (proportional to  $C^2$ ). The inverse-based constraint in line 3 also introduces extra cost in estimating the inverse norm. A brute-force implementation leads to  $O\left(\sum_{i \in \text{nnz}(\hat{\ell})} \text{nnz}(\ell_i^T)\right)$  cost in the worst case, which can be improved to  $O\left(\text{nnz}(\hat{\ell}) \log(\text{nnz}(\hat{\ell})) + \text{nnz}(\ell_r^T)\right)$  if we sort  $\hat{\ell}$  first and then estimate the inverse norm only once. Finally, with the FACSC data structure, interchanging the  $k$ th row and the  $r$ th row in  $L$  can be done in  $O(1)$  (or more precisely,  $O(C^2)$ ) operations. Therefore, the time complexity is bounded by constant per row interchange in rook pivoting. Since we limit the maximum number of row and column interchanges in rook pivoting by a constant, the total operations in rook pivoting is no greater than that of the fan-in update in ILU, and hence rook pivoting does not increase the overall time complexity.